REPORT DOCUMENTATION PAGE	Form Approved OMB No. 0704-0188

1. AGENCY USE ONLY *(Leave blank)*	2. REPORT DATE	3. REPORT TYPE AND DATES COVERED
	15.Sep.03	MAJOR REPORT

4. TITLE AND SUBTITLE
"AN EVALUATION OF MESOSCALE MODEL BASED MODEL OUTPUT STATISTICS DURING THE 2002 OLYMPIC AND PARALYMPICS WINTER GAMES"

5. FUNDING NUMBERS

6. AUTHOR(S)
MAJ HART KENNETH A

7. PERFORMING ORGANIZATION NAME(S) AND ADDRESS(ES)
UNIVERSITY OF UTAH

8. PERFORMING ORGANIZATION REPORT NUMBER
CI02-1281

9. SPONSORING/MONITORING AGENCY NAME(S) AND ADDRESS(ES)
THE DEPARTMENT OF THE AIR FORCE
AFIT/CIA, BLDG 125
2950 P STREET
WPAFB OH 45433

10. SPONSORING/MONITORING AGENCY REPORT NUMBER

11. SUPPLEMENTARY NOTES

12a. DISTRIBUTION AVAILABILITY STATEMENT
Unlimited distribution
In Accordance With AFI 35-205/AFIT Sup 1

12b. DISTRIBUTION CODE

13. ABSTRACT *(Maximum 200 words)*

DISTRIBUTION STATEMENT A
Approved for Public Release
Distribution Unlimited

20030923 121

14. SUBJECT TERMS	15. NUMBER OF PAGES
	47
	16. PRICE CODE

17. SECURITY CLASSIFICATION OF REPORT	18. SECURITY CLASSIFICATION OF THIS PAGE	19. SECURITY CLASSIFICATION OF ABSTRACT	20. LIMITATION OF ABSTRACT

THE VIEWS EXPRESSED IN THIS ARTICLE ARE THOSE OF THE AUTHOR AND DO NOT REFLECT THE OFFICIAL POLICY OR POSITION OF THE UNITED STATES AIR FORCE, DEPARTMENT OF DEFENSE, OR THE U.S. GOVERNMENT

An Evaluation of Mesoscale Model Based Model Output Statistics (MOS) During the 2002 Olympic and Paralympic Winter Games

Kenneth A. Hart*, W. James Steenburgh, Daryl J. Onton+, and Andrew J. Siffert#

NOAA Cooperative Institute for Regional Prediction and Department of Meteorology,
University of Utah, Salt Lake City, Utah

Submitted to *Weather and Forecasting*
10 April 2003
Initial revision: 29 August 2003

---

*Additional affiliation: U. S. Air Force

+Current affiliation: National Weather Service Forecast Office, Flagstaff, AZ

#Current affiliation: ACE USA, Philadelphia, PA

Corresponding author address:
Kenneth A. Hart
Department of Meteorology
135 South 1460 East Room 819
Salt Lake City, UT 84112-0110
khart@met.utah.edu

Abstract

The skill of a mesoscale model based Model Output Statistics (MOS) system that provided hourly forecasts for 18 sites over northern Utah during the 2002 Winter Olympic and Paralympic Games is evaluated. The MOS system was developed using three winters (November–April 1998–99, 1999–2000, 2000–01) of forecasts by the Pennsylvania State University/National Center for Atmospheric Research Mesoscale Model MM5 and observations from Olympic venues and transportation corridors.

MOS temperature, relative humidity, wind speed, and wind direction forecasts were considerably more accurate than those produced by the 12- and 4-km MM5. A primary contributor to MM5 temperature and relative humidity errors was a systematic overprediction of surface temperature (i.e., a warm/dry bias) during persistent and nocturnal cold-pool events when corresponding errors in MM5 dewpoint temperature forecasts were not observed. MOS largely corrected for this temperature bias. MOS wind speed forecasts outperformed the 12- and 4-km MM5 forecasts by the largest margin at locations with the lowest wind speed variability. Raw model and MOS performance exhibited minimal sensitivity to variations in model initial and lateral boundary conditions (derived from the forecasts of either the National Center for Environmental Prediction's Eta model or Aviation run of the Global Spectral Model). MOS temperature, relative humidity, and wind speed forecasts were equally or more skillful than human-generated forecasts produced by the Olympic Forecast Team.

The results illustrate that statistical techniques continue to improve upon purely numerical predictions even at high resolution. This is particularly true in a region of complex terrain where detailed characteristics of local topography and microclimates remain unresolved. It is recommended that traditional MOS or other statistical techniques based on high-density surface observations available from the MesoWest cooperative networks be used to improve gridded forecast products created by the National Weather Service Interactive Forecast Processing System (IFPS) and other applications.

1. Introduction

Weather-sensitive organizations and individuals frequently desire temporally detailed, point-specific forecasts. Such forecasts provide a unique challenge in areas of complex terrain where meteorological conditions exhibit dramatic spatial variability due to local topographic effects. Over the western United States, for example, dramatic temperature, wind speed, and wind direction differences are found over distances as small as a few tens of meters (e.g., Whiteman 1990, 2000; Doran et al. 2002; Lazarus et al. 2002), and large contrasts in precipitation are commonly observed across distances of a few kilometers (e.g., Rangno 1986; Schultz et al. 2002). As a result, forecasts for transportation corridors or areas (e.g., a ski resort) must describe a wide range of meteorological conditions.

The 2002 Olympic and Paralympic Winter Games, which were held in Salt Lake City and the adjacent Wasatch Mountains, provided several challenges of the type described above. During the Games, Olympic Forecast Team meteorologists were responsible for providing nowcast, short-range, and medium-range forecasts for five outdoor venues and six transportation corridors (Horel et al. 2002a). End users included venue managers, sports managers, transportation planners, athletes, and athletic support teams. At most venues, local topographic effects made it necessary to predict a wide range of meteorological conditions. For example, at Snowbasin ski area, considerable variability in surface weather was found along the men's downhill course, which began on a meridionally oriented ridge, traversed a zonally oriented ridge, and crossed slopes with eastern, northeastern, and southeastern exposure while falling 900 vertical meters. Wind, air temperature, and snow temperature exhibited considerable variability along the course depending on the prevailing synoptic, mesoscale, and local weather conditions.

The 12-km grid spacing of the National Centers for Environmental Prediction (NCEP) Eta model, which was available to Olympic forecasters on a 40-km grid, and the 4-km grid spacing of the real-time Pennsylvania State University/National Center for Atmospheric Research Mesoscale Model MM5 provided by the University of Utah (Horel et al. 2002a), could not accurately capture local effects of the type described above. In fact, the resolution necessary to explicitly resolve the

influence of ridges, canyons, and other topographic features on local meteorology will not likely be obtainable for many years. Even if sufficient computer power were available to explicitly resolve fine-scale topographic details, considerable improvement is needed to existing models to accurately simulate local boundary layer structure and evolution (e.g., Doran et al. 2002). As a result, current models exhibit systematic biases that limit their application toward detailed point-specific forecasting (e.g., Mass et al. 2002; Mass 2003).

One approach that has been used for more than three decades to produce objective, point-specific forecast guidance from relatively coarse resolution numerical model output is Model Output Statistics (MOS, Glahn and Lowry 1972). Currently, MOS based on the Eta Model and Aviation (AVN) run of the Global Spectral Model provides forecasts in the United States for about 1300 and 1400 sites, respectively. Unfortunately, the majority of western U.S. MOS sites are located at valley airports and are of limited utility for weather prediction in adjacent mountainous regions.

Primary forecasting responsibilities during the Games were shared by the National Weather Service (NWS) and KSL, the local National Broadcasting Company television affiliate (Horel et al. 2002a). Five forecasters from other NWS Weather Forecast Offices (WFOs) and one forecaster from the National Severe Storms Lab were selected to supplement the NWS WFO at Salt Lake City. Among other responsibilities, including warning and forecast coordination and fielding media inquiries, the supplementary NWS forecasters issued forecasts of weather, wind, temperature, wind chill, and precipitation type and amount for the primary transportation corridors twice daily for 12 locations. As part of their training, supplementary NWS forecasters issued practice transportation corridor forecasts for the World Cup events held in northern Utah in February–March 2001. The KSL forecast team, responsible for forecasting at the five outdoor venues, was composed of 13 private-sector meteorologists with extensive forecasting experience in northern Utah (Horel et al. 2002a). Venue forecast parameters included sky cover, precipitation type and amount, air temperature, wind direction, wind speed, wind gusts, wind chill, visibility, humidity and snow temperature. Assembled in 1999, venue forecasters received training during

pre-Olympic and World Cup testing and training events held over two winters prior to the Olympics. Together, the supplementary NWS forecasters and KSL venue forecasters represented the primary forecasting arm of the Olympic Forecast Team.

This paper describes and evaluates mesoscale model based MOS forecasts that were used for fine-scale weather prediction during the 2002 Olympic and Paralympic Winter Games. The MOS forecasts were provided for 18 low-, mid-, and high-elevation sites at Olympic venues and along transportation corridors. At some venues, such as the Snowbasin ski area, MOS forecasts were generated for multiple observing sites that were less than 1 km apart. The paper compares the accuracy of MOS to that of its parent high-resolution mesoscale model and human-generated forecasts produced by the Olympic Forecast Team and provides insight into the variability of MOS performance across a wide range of local topographic influences and meteorological conditions.

The remainder of this paper is organized as follows. The data and methods used to generate and verify the MOS forecasts are presented in the next section. An evaluation of MOS performance, including a comparison with that of the high-resolution numerical model and manual forecasts is described in section 3. A discussion of results then concludes the paper.

2. Data and Methods

MOS equations were generated for 18 sites in the Olympic region using three winters (November–April 1998–99, 1999–2000, 2000–01) of observations and mesoscale model forecasts. The sites were located at outdoor Olympic venues and along major transportation corridors, ranged in elevation from 1288–2835 m, and, despite their close geographic proximity, sampled a wide range of meteorological conditions (Table 1, Fig. 1). Observations from the 18 sites were provided by the MesoWest cooperative networks, which collect, integrate, and disseminate weather observations from more than 70 organizations in the western United States (Horel et al. 2002b). A total of eight organizations contributed the data used for this study, with the observations collected by a heterogeneous mix of sensors that use several different averaging

and reporting intervals. For simplicity, all observations within 30 min of the top of each hour were averaged to generate a more homogeneous dataset for MOS development, implementation, and validation. A simple gross-range-check algorithm was used to eliminate clearly erroneous observations. For example, relative humidity was constrained to be from 0.1 to 100%, temperature from -70 to 135°F (-56.7 to 57.2°C), dewpoint from -90 to 100°F (-67.8 to 37.8°C), wind speed from 0 to 200 m s^{-1}, and wind direction from 0 to 360°. No additional quality checks were attempted. MOS equations were not developed for precipitation because a longer period of record was required to fully sample the large variability of precipitation events.

Mesoscale model forecasts were provided by a real-time version of the MM5 (Grell et al. 1994) that was run at the University of Utah (Horel et al. 2002a). During the three winter MOS equation development period, the real-time MM5 featured two domains with 36- and 12-km grid spacing. Forecasts produced by the 12-km domain were used for MOS equation development. Although changes were made to the MM5 during the equation development period, no efforts were made to account for these changes in the MOS equations, as is done with updatable MOS (e.g. Wilson and Vallée 2002). Early tests suggested that traditional MOS produced adequate performance (Siffert 2001), in agreement with the findings of Wilson and Vallée (2002) who found that MOS forecast equations remained remarkably stable despite changes in the driving model. MM5 changes during the development period included an upgrade from MM5 version 2 to MM5 version 3, migration of the modeling system from an SGI Origin 2000 to a PC-based Linux cluster, expansion of the 12-km domain, the addition of a 4-km domain, and incorporation of high-density MesoWest surface observations into the initial analysis provided by the NCEP Eta model (Horel et al. 2002b; Lazarus et al. 2002). To limit the impact of these changes on MOS performance, the topography of the 12-km domain was not changed over the Olympic region and feedback from the 4-km domain to the 12-km domain was not allowed. Throughout the MOS development and Olympic forecast periods, the real-time MM5 featured the convective, radiative, boundary layer, and microphysical parameterizations described by Kain and Fritsch (1993), Dudhia (1989), Hong and Pan (1996), and Dudhia (1989), respectively. Additional information

concerning the real-time MM5 is provided by Horel et al. (2002a).

Following Glahn and Lowry (1972) and Glahn (1985), separate MOS equations were developed for each site, model cycle (0000 and 1200 UTC), variable, and forecast hour at 3-h intervals (e.g., 3, 6, 9,...36 h) using forward–stepwise multivariate linear regression. Hourly forecasts were then generated by weighting the 3-h coefficients in time. For example, a 7-h forecast equation reflected 2/3 influence from the 6-h forecast equation and 1/3 influence from the 9-h equation. Predictands (i.e., the variables that were being predicted) were temperature, dewpoint, relative humidity, wind speed, zonal wind and meridional wind for the sensor level. MOS wind direction was derived from the zonal and meridional wind components. Note that MOS relative humidity was not derived from MOS temperature and dewpoint forecasts, but was based on its own forecast equations since early work suggested such an approach was more accurate. Predictors (i.e., variables that may be related to each predictand) included MM5 model forecast variables (interpolated to the station location), geoclimatic predictors, and surface observations (Table 2). For simplicity, only predictors at the forecast hour for which the equation was being developed were used in each equation. Geoclimatic predictors consisted of sine and cosine of the normalized day of the year. Surface observations included observations 3 h after the MM5 initialization time and observations, used as persistence predictors, valid at the time of the forecast. Since equipment or network failures can result in observational data outages, secondary equations that excluded prior surface observations were developed and used when prior observations were not available. A commercial software package, JMP™ (Sall et al. 2001), was used to perform the forward–stepwise multivariate linear regression. The default JMP™ stopping criteria, which is based on the Wilk's Lambda, Pillai's Trace, Hotelling-Lawley Trace, and Roy's Max Root statistical tests (Sall et al. 2001), was used to determine when to stop adding potential predictors. Using this approach, MOS equations typically consisted of about 15 predictors, similar to that of NGM MOS (Jacks et al. 1990).

Unless otherwise indicated, results presented in this paper are based on hourly forecasts and observations from 23 January – 24 March 2002, which encompassed the Olympic (8–26

February) and Paralympic (7–16 March) Games. For the purpose of this evaluation, the 18 verification sites were separated into three groups based on terrain characteristics: mountain, mountain valley, and Wasatch Front (Table 1, Fig. 1). Elevations at the seven mountain sites in the Wasatch Mountains ranged from 2146 to 2835 m. Five mountain valley sites, located in valleys to the east of the Wasatch Mountains, were characterized by elevations from 1689 to 2000 m. The remaining six locations, classified as Wasatch Front sites with elevations from 1288 to 1498 m, were located in the lowlands immediately west of the Wasatch Range. Raw model output from the MM5 12- and 4-km domains was verified based on interpolation of grid-point forecasts to the positions of the observing sites.

Since the MOS forecasts during the Games were not archived, the results were based on applying the MOS equations to archived MM5 forecasts. In general, the resulting MOS forecasts should be the same as those available to Olympic forecasters, although it is possible that, because of the arrival of late observations, primary equations were used at a few times that the Olympic forecasters would have had access to a forecast generated by a secondary equation.

Accuracy measures used were the bias error (BE) and mean absolute error (MAE). The BE represents the model tendency to overforecast or underforecast the observed quantity (Wilks 1995) and is defined as:

$$BE = \frac{1}{N} \sum_{i=1}^{N} (f_i - o_i)$$

where N is the number of forecast/observation pairs in the sample, f_i is the forecast and o_i is the observation. Negative (positive) BE values indicate underforecasting (overforecasting). The MAE indicates the average magnitude of the forecast error and is defined as:

$$MAE = \frac{1}{N} \sum_{i=1}^{N} |f_i - o_i|$$

Forecasts produced by the 12-km MM5, 4-km MM5, and MOS were also compared to those of the Olympic Forecast Team. This involved the use of a smaller set of data corresponding to the variables and periods for which the Olympic Forecast Team provided forecasts. For transportation corridors, temperature forecasts produced from 3–25 February and 7–16 March were examined for five locations (Table 1). Temperature, relative humidity, and wind speed forecasts produced from 1–24 February were also considered for five outdoor venues (Table 1).

3. Results

a. Temperature forecasts

Averaged over all locations, there was little difference in the performance of the 12- and 4-km MM5, with temperature MAEs of 3.27 and 3.21°C, respectively (Fig. 2). MOS was substantially more accurate, with a mean absolute error of only 1.71°C, a reduction of over 40% compared to the direct model output. MAEs for the 12-km MM5, 4-km MM5, and MOS were largest at mountain valley sites. MOS errors were smallest at mountain sites, whereas the 12- and 4-km MM5 performed best at Wasatch Front sites.

One possible contributor to MM5 errors was differences between model and actual elevation. In an effort to determine the impact of such errors, 12- and 4-km MM5 temperatures were adjusted to the actual station elevation by assuming a U.S. standard atmosphere lapse rate of 6.5°C km^{-1}. Mass et al. (2002) used this approach in their evaluation of MM5 forecasts over the Pacific Northwest. While this adjustment improved the performance at higher elevation mountain locations, it either degraded or provided little improvement at Wasatch Front and mountain valley locations (Fig. 2). Causes for this degraded performance and possible implications for producing graphical forecast products are discussed later in the paper.

A major contributor to MM5 temperature errors during the validation period was an inability to simulate cold pool strength and evolution properly. Cold pools are topographically confined layers of air that are colder than layers immediately above, and can be characterized as either diurnal (i.e., nocturnal) or persistent (i.e., multiday) based on their duration (Whiteman et

al. 2001). Persistent cold pools, characterized by unusually cold temperatures and limited boundary layer mixing, were present over the Wasatch Front from 28 January – 16 February, with a brief period of well-mixed conditions on 8 February accompanying the passage of a cold front. The temperature MAE time series[1], illustrates that consistently large errors were produced by the 12- and 4-km MM5 during the cold pool periods (Fig. 3a). In contrast, MOS errors were much smaller and typical of the Olympic and Paralympic periods as a whole. In general, MOS errors were more consistent throughout the two-month period. A time series of the temperature bias error indicates that the 12- and 4-km MM5 exhibited a large warm bias (~3–4°C) during the persistent cold-pool events (Fig. 3b).

With the exception of two mountain sites, the 12- and 4-km MM5 temperature MAEs were generally larger for stations with larger mean diurnal temperature cycles (Figs. 4a,b). Large contrasts between model and actual elevation were responsible for the anomalously high temperature MAEs at the two mountain sites. Adjusting model temperatures using a standard atmospheric lapse rate largely removed this error, moving the two mountain stations closer to a least-squares fit line [the standard atmospheric lapse rate adjustment for temperature worked best for sites dominated by free-atmospheric temperatures (i.e., mountain sites)]. MOS temperature MAEs were smaller than those of the 12- and 4-km MM5 (Fig. 2), particularly for stations with larger mean diurnal temperature cycles where MOS added the greatest value (Fig. 4c).

The 12- and 4-km MM5 temperature MAEs were largest during the evening, overnight, and early morning hours (0000–1400 UTC) and smallest during the day (1400–0000 UTC) (Fig. 5a). As a result, MM5 errors did not increase monotonically with time, although for the 0000 UTC (1200 UTC) initialized MM5 forecasts, errors during the second nighttime (daytime) period were larger than the first, illustrating that model temperature errors grow with increasing forecast projection. MOS MAEs exhibited monotonic error growth at night, and little or no growth during

[1] MAE and BE time series plots for the validation period are based on errors averaged for each model run at all forecast hours (3–36 every 3 h) for all 18 sites.

the day.

The 12- and 4-km MM5 forecasts produced a large (2–3°C) warm bias during the night hours, suggesting that the model was unable to properly simulate the strength of nocturnal cold pools or stable layers (Fig. 5b). This warm bias was a major contributor to the large nighttime MAEs evident in Fig. 5a. During the day, relatively small (~1°C or less) 12- and 4-km MM5 temperature bias errors were observed. The 12-km MM5 elevations were, on average, 100 m higher than the 4-km MM5 elevations at valley locations. As a result, the colder 12-km MM5 temperatures resulted in less bias than the 4-km MM5 since valley locations were often under the influence of nocturnal or persistent cold pools. 12- and 4-km MM5 nighttime warm biases were reduced from 2–3°C to 1°C by MOS. The large (2–3°C) MM5 nighttime warm bias found in the present study contrasts with the smaller (~1°C) bias errors reported by Mass et al. (2002) in a verification study of a comparable resolution MM5 modeling system over the Pacific Northwest. Less cloud cover and more well-developed diurnal cold pools may help explain the larger nocturnal warm bias produced by the MM5 over northern Utah.

b. Dewpoint forecasts

Unlike temperature, the 12- and 4-km MM5 dewpoint MAEs during the persistent cold pool episodes were typical of the Olympic and Paralympic periods (Fig. 6a). While MOS dewpoint errors were less than the 12-km and 4-km MM5 throughout the period, the value added by MOS was not substantially larger during the persistent cold pool episodes. No significant BE was observed with the 12- and 4-km MM5 dewpoint forecasts (0.27 and -0.38°C, respectively) (Fig. 6b). Overall, MOS overpredicted (higher than observed) dewpoint values for the 61-day period by 1.25°C. The largest dewpoint MAEs for the 12- and 4-km MM5 occurred during the afternoon hours (1900–2300 UTC) (Fig. 7a). Once again, MOS errors were less than raw model errors at all hours. Most of the MM5 error during the afternoon was associated with a significant dry bias, with minimal dewpoint bias overnight (Fig. 7b).

c. Relative humidity forecasts

Relative humidity MAEs for the 12- and 4-km MM5 were 16% and 18%, respectively (Fig. 8). The comparatively worse performance of the 4-km MM5 may be related to temperature errors associated with model elevation errors as described in section 3a. MOS significantly outperformed the MM5 with a relative humidity MAE of ~10%. The greatest improvement by MOS over the MM5 was found at mountain valley locations, whereas the smallest improvement was for the mountain sites.

Like temperature, the 12- and 4-km MM5 relative humidity MAEs were consistently higher during the two persistent cold pool events (Fig. 9). This might be expected since, during the cold events, neither the 12- or 4-km MM5 accurately depicted the observed temperature (Fig. 3), which is used to determine the relative humidity. Episodes where the MM5 relative humidity MAEs were as large as those found during the persistent cold pool events also occurred later in the Olympic period, and maxima in MOS relative humidity MAEs were also evident during these periods (e.g., 5–6 March and 22–23 March). Since MOS largely corrects for systematic model biases, poor model and MOS performance during these periods may be a reflection of more random model errors that arise from the poor placement and/or amplitude of synoptic and mesoscale systems.

The 12- and 4-km MM5 relative humidity MAEs were largest at night, particularly from 0500–1500 UTC (Fig. 10a). MOS errors were less than the 12-km and 4-km MM5 at all hours and exhibited a more modest diurnal modulation. The relative humidity bias errors shown in Fig. 10b indicate that the 12- and 4-km MM5 were too dry, particularly at night. Since relative humidity is a function of both temperature and moisture, the strong overnight dry bias in relative humidity is most likely associated with errors in model temperature that result from the inability of the model to properly develop nocturnal cold pools. Causes for the larger dry bias in the 4-km MM5 may, again, be the result of the larger 12-km MM5 elevation errors that led to colder and, consequently, more accurate 12-km temperature forecasts during cold pool episodes. MOS bias errors were less than 5%. Overall, these results further illustrate the inability of the MM5 to properly simulate the

structure of persistent and diurnal cold pools and stable layers.

d. Wind forecasts

Averaged over all stations, MOS wind speed MAEs were substantially lower (~1 m s^{-1}) than those of the 12- and 4-km MM5 (3.3 and 3.2 m s^{-1}, respectively), a reduction in error of over 65% (Fig. 11a). Although one might expect that there would be substantial improvement in wind speed skill with decreasing grid spacing, the 4-km MM5 forecast error was only marginally better than that of the 12-km MM5. At mountain valley locations, where the 12- and 4-km wind speed MAEs were the largest, MOS added the greatest value and featured very small MAEs. Wind direction MAEs for the 12- and 4-km MM5, calculated for periods when wind speeds were at least 2.5 m s^{-1}, were 59 and 57°, respectively (Fig. 11b). MOS reduced these wind direction errors by 30% overall, with the greatest improvement found at mountain locations and only limited improvement evident at mountain valley and Wasatch Front sites.

There was a modest diurnal modulation of 12- and 4-km MM5 wind speed MAE with the largest error during the night and early morning hours (Fig. 12a). This was likely related to the aforementioned problem simulating nocturnal cold pool structure. The 12- and 4-km MM5 overpredicted wind speeds, particularly during the overnight hours (Fig. 12b). There was no significant diurnal variability or overall bias, however, associated with wind speeds produced by MOS.

Of the variables examined in this study, wind speed and direction exhibit the greatest amount of spatial variability and are very sensitive to the topographic and land-surface characteristics of each observing site. This is particularly true of MesoWest observations, which for this study, were provided by eight different networks designed for the needs of their operating agency or group. Some observing sites, including Deer Valley-Burns (DVE), Snowbasin-Base (SBE), Park City Golf Course (SNC) and Utah Olympic Park-Upper Bear (WBU), were installed to collect precipitation and were located in well-sheltered areas with limited wind exposure. As a result, wind speed magnitude and variability at these locations was typically lower than that found

at other MesoWest sites.

The 12- and 4-km MM5 wind speed MAEs were largest for sites with small observed wind speed standard deviations (Figs. 13a,b). At these sites, the grid-cell averaged wind produced by MM5 was not representative of the unique local conditions at the observing sites. Smaller MAEs were found at more exposed sites that exhibited greater variability. In contrast, MOS MAEs grew with increasing wind speed standard deviation (Fig. 13c). In other words, as the variability of the observations increased, MOS performance decreased. At locations where there was less wind speed variability, MOS outperformed the 12- and 4-km MM5 by a large margin because it corrected for the unique local conditions at these observing sites. At more exposed sites, such bias corrections were smaller and the larger MOS MAEs were a reflection of the greater variability and lower predictability of wind speed. These results also suggest that the influence of terrain and land-use heterogeneities on local wind observations should be considered when performing model verification studies, particularly in mountainous regions.

e. Variations in initial conditions

The results described above were based upon MM5 simulations whose initial conditions were provided by the NCEP Eta model initial analysis, which was enhanced at low-levels based on high-density surface observations provided by the MesoWest cooperative networks (Horel et al. 2002b). During the Olympic and Paralympic periods, a second simulation using the NCEP AVN model for the initial condition first guess was run at each initialization time. These simulations were referred to as MM5-Eta and MM5-AVN, respectively. The MOS equations developed for the MM5-Eta were also applied to the MM5-AVN, providing an opportunity to examine the variability of MOS performance produced by differing initial conditions.

Figure 14 presents the 36-h temperature, relative humidity, and wind speed MAEs from the MM5-Eta MOS, MM5-AVN MOS, and the forecast obtained by averaging the MM5-Eta and MM5-AVN MOS predictions (consensus MOS). The 36-h forecasts were considered independently to allow for the greatest potential of divergent solutions. There was remarkably

little sensitivity of MOS errors during this period to differences in the initial and lateral conditions provided by the NCEP Eta and AVN models (Fig. 14). Strong local forcing mechanisms resulting from the complex terrain of northern Utah may have limited the effect of lateral boundary condition errors, or limited area model simulations based on small perturbations in initial conditions may not have produced solutions that diverge like those of an unbounded model (Warner et al. 1997). The consensus MOS performance exhibited no significant improvement over the individual performance of MM5-Eta MOS or MM5-AVN MOS (Fig. 15). Similar results were obtained for relative humidity and wind speed (not shown). In contrast, Vislocky and Fritsch (1995) found that the consensus MOS forecasts calculated from two different models (e.g. NGM and LFM) improved performance over MOS forecasts from individual models. In the present study, perhaps the limited sensitivity of the MM5 to Eta and AVN initial conditions limits the value added by consensus MOS.

f. Comparison with Olympic Forecast Team transportation route and outdoor venue forecasts

The Olympic Forecast Team issued transportation corridor forecasts twice daily at ~2300 UTC (the PM forecast) and ~1200 UTC (the AM forecast), including temperature forecasts valid at 1500, 1900, and 2300 UTC for the five MOS sites identified in Table 1. MM5 and MOS errors are presented for the model run used by the Olympic Forecast Team in producing their forecast (e.g., the 1200 UTC initialized MM5 for the PM forecast) and the model run corresponding to the time the Olympic Forecast Team issued their forecast (e.g., 0000 UTC for the PM forecast) (Fig. 16). Forecast projections for the 1200 and 0000 UTC model runs compared for the PM forecast issuance were 27/31/35 h and 15/19/23 h, respectively. For the PM forecast, the Olympic Forecast Team temperature MAEs (2.9°C) were comparable to those of the 12- and 4-km MM5 for both the model run available to forecasters (1200 UTC) and the model run initialized at the time they issued their forecast (0000 UTC). MOS errors were, however, considerably smaller (~2°C), about 1°C less than those of the Olympic Forecast Team.

For the AM forecasts, a more complex picture emerges. Forecast projections for the 0000

and 1200 UTC model runs compared for the AM forecast issuance were 15/19/23 h and 7/11 h, respectively[2]. Olympic Forecast Team temperature MAEs (2°C) were about 1°C smaller than the 0000 UTC initialized 12- and 4-km MM5 that was available for producing their forecast, and comparable to the 0000 UTC initialized MOS (~2°C). The improvement over the 1200 UTC 12-km and 4-km MM5, initialized at the time the Olympic Forecast Team forecast was issued, was smaller. The 1200 UTC initialized MOS MAEs were 18% smaller than those of the Olympic Forecast Team.

From 1–24 February, the Olympic Forecast Team also issued forecasts for five Olympic venue locations (Table 2). For this period, Olympic Forecast Team forecasts of temperature, relative humidity and wind speed, issued for 3-h intervals through 36 h at ~0000 UTC (the PM forecast) and ~1200 UTC (the AM forecast), were compared to the 12-km MM5, 4-km MM5 and MOS forecasts (Fig. 17). As with the transportation corridor forecasts, MM5 and MOS MAEs are presented for the model runs used by the Olympic Forecast Team in producing their forecast and the model run corresponding to the time that the Olympic Forecast Team issued their forecast. For the PM forecast, Olympic Forecast Team temperature MAEs (2.4°C) were significantly smaller than those of the 12- and 4-km MM5 for both the model run available to forecasters (1200 UTC) and the model run initialized at the forecast issue time (0000 UTC) (Fig. 17a). MOS temperature MAEs for the model run available to forecasters (1200 UTC, 1.8°C) were smaller, however, than Olympic Forecast Team temperature MAEs. MOS temperature MAEs for the model run initialized at the time of forecast issue were even smaller (0000 UTC, 1.6°C). For the AM forecast, a similar result emerged. Olympic Forecast Team MAEs (2.1°C) were significantly less than those of both 12- and 4-km MM5 runs, but larger than MOS temperature MAEs for the model run available to forecasters (0000 UTC, 2.0°C) and the model run initialized at the time of forecast issue (1200 UTC, 1.5°C), although the difference was not as large as found for the PM

[2] Since 1200 UTC MOS uses the 1500 UTC temperature as a predictor, the AM forecast comparison for 1200 UTC products did not use the temperature forecast valid at 1500 UTC and is based only on the 7-h and 11-h forecasts valid at 1900 and 2300 UTC.

forecasts. Similarly, for both relative humidity (Fig. 17b) and wind speed (Fig. 17c), MOS MAEs were comparable or smaller than those of the Olympic Forecast Team.

The lower MAEs of MOS forecasts compared with those of the Olympic Forecast Team may be surprising since many National Weather Service forecasters improve upon NGM and AVN MOS forecasts. For example, at the Salt Lake City forecast office from 1 December 2001 – 31 March 2002, human forecasts of maximum and minimum temperature at the Salt Lake City International Airport (SLC) and Cedar City Airport (CDC) featured a MAE of 1.99°C, compared with 2.36 and 2.17°C for NGM MOS and AVN MOS, respectively (M. E. Jackson, personal communication). The Olympic forecasts, however, featured considerably more detail than maximum and minimum temperature forecasts for two sites and included predictions for multiple variables at frequent time intervals, many of which are not presented in this study. In the case of the Olympic venue forecasts, temperature, relative humidity, and wind speed predictions were verified at 3-h intervals. Thus, the lower skill of the Olympic Forecast Team forecasts compared with MOS may be a reflection of the difficulties of predicting a large number of variables at frequent intervals. It is also possible that the relatively brief Olympic period did not feature weather regimes where the Olympic Forecast Team forecasters could improve substantially upon MOS.

4. Implications for IFPS and the future role of human forecasters

The results presented above have a number of implications for operational weather prediction over the western United States, particularly in an era where the National Weather Service will prepare and disseminate gridded forecast products based on the Interactive Forecast Preparation System (IFPS, Glahn and Ruth 2003). First, for the sites examined in this paper, decreasing model grid spacing from 12- to 4-km produced only marginal improvement in the prediction of surface temperature, wind speed, and wind direction, and actually degraded the surface relative humidity forecast. This suggests that increasing the resolution of a numerical model to match the proposed 2.5-km grid spacing of IFPS forecasts issued by the National

Weather Service Western Region, as suggested by Mass (2003), will likely provide little, if any, improvement over guidance provided by existing coarser resolution models such as the 12-km Eta model. Second, it appears that some simple downscaling techniques, such as adjusting model temperatures for model and actual elevation differences using a U.S. standard atmosphere, may produce only marginal forecast improvements and, in some situations, such as when persistent or diurnal cold-pools are present, actually degrade the forecast. While the assumed lapse rate can be adjusted in IFPS on a case by case basis, the considerable spatial variability in cold-pool strength and depth will make this a daunting task to perform accurately over an entire county warning area.

Perhaps the most important result is the dramatic gain in forecast accuracy produced using traditional MOS. Clearly, the ability to account and correct for systematic biases produces substantially larger forecast improvements than can be obtained by decreasing the horizontal grid spacing of existing models. Although improvements in observing technologies, data assimilation, and model numerics and physics will result in more accurate numerical forecasts with smaller biases in the future, it will likely take many years until model forecasts can be accurately applied to the prediction of surface weather variables.

Although it is possible to produce a gridded forecast using NGM, AVN, or Eta MOS with IFPS, the limited number and predominant valley siting of western U.S. MOS sites limits the utility of such forecasts. There is, however, a new possibility – applying MOS or other statistical techniques using high-density observations provided by the MesoWest cooperative networks and other non-conventional networks.

Presently, MesoWest collects data from more than 3500 stations in the western United States (Horel et al. 2002b). Observations span all elevations because of contributions from organizations with meteorological sensors in valley locations (e.g., air quality and transportation agencies) and at high elevations (e.g., Bureau of Land Management and ski resorts). In some regions, data density is very high. For example, over northern Utah, data is collected from more than 250 sites (Horel et al. 2002b). A substantial historical record of many sites is available and could be applied for MOS equation development based on the Eta model and the Global Forecast

System. Other postprocessing approaches, such as Kalman filters (e.g., Homleid 1995; Majewski 1997), neural networks (Hsieh and Tang 1998), and Group Method of Data Handling (GMDH) algorithms (e.g., Abdel-Aal and Elhadidy 1995), could also be used and possibly take advantage of output from ensemble modeling systems.

The need to utilize MesoWest or other high-density observing networks to produce more accurate gridded forecasts is further illustrated by the fact that MOS temperature, relative humidity, and wind speed MAEs were comparable to or smaller than those of the Olympic Forecast Team. This illustrates how difficult it is for humans to produce forecasts for a large number of variables at high temporal resolution and suggests that the development of MesoWest-based MOS would result in more accurate gridded first-guess fields for forecaster manipulation, and, in turn, better forecasts for the western United States. In addition, a more accurate first-guess field would also allow the forecaster to focus on other important components of the forecast process including short-term forecasts, subjective evaluation of model analyses and forecasts, and communicating the forecast to the public (Mass 2003).

One significant obstacle that remains, however, concerns how to use irregularly spaced, point-specific MesoWest-based MOS to produce a gridded forecast. In particular, how could an accurate forecast be produced for data sparse areas? Given the wide range of terrain geometries, how can one best interpolate the point forecasts to the grid? Should anisotropic weighting functions be used, as proposed by Lazarus et al. (2002)? Finally, for fields like wind speed and direction, how will local terrain and land-use heterogeneities be considered? In addition, the small number of precipitation sites limits the ability to apply MesoWest observations for statistical correction of model precipitation forecasts. Clearly, issues remain for applying IFPS in the most efficient and effective manner.

5. Conclusions

This paper has examined the performance of a mesoscale model based MOS system that provided forecasts for 18 sites over northern Utah during the 2002 Olympic and Paralympic

Games. MOS forecast accuracy was compared with direct output of the 12- and 4-km MM5 forecasts, as well as with that of the Olympic Forecast Teams.

Decreasing model grid spacing from 12 to 4 km produced marginal or no improvement in the prediction of surface temperature, relative humidity, wind direction, and wind speed. In contrast, MOS provided substantially better temperature, wind, and moisture forecasts. Large MM5 temperature forecast errors were produced at valley locations due to the poor handling of nocturnal inversions and persistent cold pool events. These temperature forecast errors led to a dry relative humidity bias during the same periods. MOS reduced these errors by correcting for MM5 warm biases during such stable periods. MOS added more value to wind forecasts at locations where there was the lowest observed wind speed variability. Variations in model initial and lateral boundary conditions (e.g. Eta or AVN) did not significantly affect raw model or MOS performance. MOS temperature, relative humidity and wind speed MAEs at Olympic outdoor venue and transportation corridor sites were comparable to or smaller than those of the Olympic Forecast Team, highlighting the human challenges associated with forecasting multiple variables for high temporal resolutions.

These results suggest that statistical techniques can account for and correct systematic biases and improve upon purely dynamical predictions, even at fine grid spacings. With the development of high-density surface observation networks across the Western United States (e.g., MesoWest), where detailed characteristics of local topography and microclimates remain unresolved, traditional MOS or other statistical forecast techniques should be incorporated into IFPS and other applications to produce more accurate gridded forecasts than can be obtained by downscaling direct model output to high-resolution grids.

Acknowledgements. This work was sponsored by a series of grants provided by the National Weather Service C-STAR program to the NOAA Cooperative Institute for Regional Prediction at the University of Utah. Larry Dunn, John Horel, Jan Paegle, Mark Jackson, Brett McDonald, Will Cheng, Dave Schultz, and two anonymous reviewers provided insightful

discussion and comments that enhanced and improved the manuscript. Computer time for the Olympic forecasts was provided by the University of Utah Center for High Performance Computing. MesoWest data were collected and processed by John Horel, Mike Splitt, Judy Pechmann, and Bryan White. We would like to thank the governmental agencies, commercial firms, and educational institutions that provide data to MesoWest. We greatly appreciate the support of Mark Eubank, KSL-TV, who provided the outdoor venue forecast data. Transportation corridor forecast data were provided by the National Weather Service forecast office at Salt Lake City. The first author gratefully acknowledges the support of the United States Air Force AFIT program during this study.

References

Abdel-Aal, R. E., and M. A. Elhadidy, 1995: Modeling and forecasting the daily maximum temperature using abductive machine learning. *Wea. Forecasting*, **10**, 310-325.

Doran, J. C., J. D. Fast, and J. Horel, 2002: The VTMX 2000 campaign. *Bull. Amer. Meteor. Soc.*, **83**, 537-551.

Dudhia, J., 1989: Numerical study of convection observed during the Winter Monsoon Experiment using a mesoscale two-dimensional model. *J. Atmos. Sci.*, **46**, 3077-3107.

Glahn, H. R., 1985: Statistical weather forecasting. *Probability, Statistics, and Decision Making in the Atmospheric Sciences*, A. H. Murphy and R. W. Katz, Eds., Westview Press, 289-335.

_____, and D. A. Lowry, 1972: The use of model output statistics (MOS) in objective weather forecasting. *J. Appl. Meteor.*, **11**, 1203-1211.

_____, and D. P. Ruth, 2003: The new digital forecast database of the National Weather Service. *Bull. Amer. Meteor. Soc.*, **84**, 195-201.

Grell, G. A., J. Dudhia, and D. R. Stauffer, 1994: A description of the fifth-generation Penn State/ NCAR Mesoscale Model (MM5). NCAR Tech. Note NCAR/TN-398+STR, 138 pp. [Available from National Center for Atmospheric Research, P.O. Box 3000, Boulder, CO 80307.]

Homleid, M., 1995: Diurnal corrections of short-term surface temperature forecasts using the Kalman filter. *Wea. Forecasting*, **10**, 689-707.

Hong, S. –Y., and H.-L. Pan, 1996: Nonlocal boundary layer vertical diffusion in a medium-range forecast model. *Mon. Wea. Rev.*, **124**, 2322-2339.

Horel, J., T. Potter, L. Dunn, W. J. Steenburgh, M. Eubank, M. Splitt, and D. J. Onton, 2002a: Weather support for the 2002 Winter Olympic and Paralympic Games. *Bull. Amer. Meteor. Soc.*, **83**, 227-240.

_____, and Coauthors, 2002b: MesoWest: Cooperative mesonets in the western United States. *Bull. Amer. Meteor. Soc.*, **83**, 211-226.

Hsieh, W. W., and B. Tang, 1998: Applying neural network models to prediction and data analysis in meteorology and oceanography. *Bull. Amer. Meteor. Soc.*, **79**, 1855-1870.

Jacks, E., B. Bower, V. J. Dagostaro, J. P. Dallavalle, M. C. Erickson, and J. C. Su, 1990: New NGM-based MOS guidance for maximum/minimum temperature, probability of precipitation, cloud amount, and surface wind. *Wea. Forecasting*, **5**, 128-138.

Kain, J. S., and J. M. Fritsch, 1993: Convective parameterizations for mesoscale models: The Kain Fritsch scheme. *The Representation of Cumulus Convection in Numerical Models, Meteor. Monogr.*, No. 24, Amer. Meteor. Soc., 165-170.

Lazarus, S. M., C. M. Ciliberti, J. D. Horel, and K. A. Brewster, 2002: Near-real-time applications of a mesoscale analysis system to complex terrain. *Wea. Forecasting*, **17**, 971-1000.

Majewski, D., 1997: Operational regional prediction. *Meteor. Atmos. Phys.*, **63**, 89-104.

Mass, C. F., 2003: IFPS and the future of the National Weather Service. *Wea. Forecasting*, **18**, 75-79.

_____, D. Ovens, K. Westrick, and B. A. Colle, 2002: Does increasing horizontal resolution produce more skillful forecasts? The results of two years of real-time numerical weather prediction over the Pacific Northwest. *Bull Amer. Meteor. Soc.*, **83**, 407-430.

Rangno, A. L., 1986: How good are our conceptual models of orographic cloud seeding? *Precipitation Enhancement-A Scientific Challenge*, R. R. Braham, Jr., Ed., *Meteor. Monogr.*, No. 43, Amer. Meteor. Soc., 115-124.

Sall, J., A. Lehman, and L. Creightin, 2001: *JMP™ Start Statistics*, SAS Institute Inc. Duxbury Thomson Learning, Pacific Grove, CA, 491 pp.

Schultz, D. M., and Coauthors, 2002: Understanding Utah winter storms: The Intermountain Precipitation Experiment. *Bull. Amer. Meteor. Soc.*, **83**, 189-210.

Siffert, A.J., 2001: Point-specific MOS forecasts for the 2002 Winter Games. M.S. thesis, Dept. of Meteorology, University of Utah, 51 pp. [Available from Dept. of Meteorology, University of Utah, 135 South 1460 East, Salt Lake City, UT 84112.]

Vislocky, R. L., and J. M. Fritsch, 1995: Improved model output statistics forecasts through model consensus. *Bull Amer. Meteor. Soc.*, **76**, 1157-1164.

Warner, T. T., R. A. Peterson, and R. E. Treadon, 1997: A tutorial on lateral boundary conditions

as a basic and potentially serious limitation to regional numerical weather prediction. *Bull. Amer. Meteor. Soc.*, **78**, 2599-2617.

Whiteman, C. D., 1990: Observations of thermally developed wind systems in mountainous terrain. *Atmospheric Processes over Complex Terrain, Meteor. Monogr.*, No. 45, Amer. Meteor. Soc., 5-42.

_____, 2000: *Mountain Meteorology: Fundamentals and Applications*. Oxford University Press, New York, 355 pp.

_____, S. Zhong, W. J. Shaw, J. M. Hubbe, X. Bian, and J. Mittelstadt, 2001: Cold pools in the Columbia Basin. *Wea. Forecasting*, **16**, 432-447.

Wilks, D. S., 1995: *Statistical Methods in the Atmospheric Sciences*. Academic Press, 467 pp.

Wilson, L. J., and M. Vallée, 2002: The Canadian Updateable Model Output Statistics (UMOS) System: Design and development tests. *Wea. Forecasting*, **17**, 206-222.

Table captions

Table 1. MM5 MOS Sites. See Fig. 1 for locations. "T" indicates a transportation corridor forecast site and "V" indicates a outdoor venue forecast site.

Table 2. MOS predictors.

Tables

Table 1. MM5 MOS sites. See Fig. 1 for locations. "T" indicates a transportation corridor forecast site and "V" indicates a outdoor venue forecast site.

Site	ID	Elev (m)	Site Type	Venue/Transportation Corridor
Deer Valley-Bald Eagle	DVB	2591	Mountain	Alpine/freestyle skiing
Deer Valley-Burns (V)	DVE	2235	Mountain	Alpine/freestyle skiing
Park City-Eagle	PCS	2610	Mountain	Alpine skiing/snowboarding
Snowbasin-Allens Pk	SBB	2835	Mountain	Alpine skiing
Snowbasin-John Paul	SBW	2670	Mountain	Alpine skiing
Utah Olympic Park-Bear Upper (V)	WBU	2182	Mountain	Ski jumping/luge/skeleton/ bobsled
Parleys Summit (T)	PSS	2146	Mountain	I-80 (mountain pass)
Park City-Base (T, V)	PCB	2000	Mountain Valley	Alpine skiing/snowboarding
Park City Municipal Golf Course	SNC	1937	Mountain Valley	Alpine skiing/snowboarding
Snowbasin-Base (V)	SBE	1925	Mountain Valley	Alpine skiing
Soldier Hollow (V)	WMP	1713	Mountain Valley	Nordic skiing/biathlon
Soldier Hollow Whales Tail	WM2	1689	Mountain Valley	Nordic skiing/biathlon
Bluffdale	UT7	1433	Wasatch Front	I-15
Hill AFB	HIF	1459	Wasatch Front	I-15/I-84
Ogden-Hinkley Airport (T)	OGD	1362	Wasatch Front	I-15/I-84
Parleys Canyon Mouth	UT5	1498	Wasatch Front	I-80
Provo (T)	PVU	1369	Wasatch Front	I-15
Salt Lake City Intl Airport (T)	SLC	1288	Wasatch Front	Aviation hub

Table 2. MOS predictors.

Predictors	Levels
MM5	
Temperature	σ = 0.995, 800 hPa, 700 hPa, 600 hPa, 500 hPa
Dewpoint	σ = 0.995, 800 hPa, 700 hPa, 600 hPa, 500 hPa
Relative Humidity	σ = 0.995, 800 hPa, 700 hPa, 600 hPa, 500 hPa
Zonal Wind Speed	σ = 0.995, 800 hPa, 700 hPa, 600 hPa, 500 hPa
Meridional Wind Speed	σ = 0.995, 800 hPa, 700 hPa, 600 hPa, 500 hPa
Total Wind Speed	σ = 0.995, 800 hPa, 700 hPa, 600 hPa, 500 hPa
Geopotential Height	800 hPa, 700 hPa, 600 hPa, 500 hPa
Vertical Velocity	800 hPa, 700 hPa, 600 hPa, 500 hPa
3-h Accumulated Precipitation	
Surface-700-hPa Lapse Rate	
Mean Surface-500-hPa Relative Humidity	
Geoclimatic	
Sine of Normalized Day of Year	
Cosine of Normalized Day of Year	
Observations	
Most recent available prior surface observation at same time of day as forecast projection	
Surface observations at 3 h after initialization time	

Figure captions

Figure 1. Geography of the Olympic region, outdoor Olympic venues, and MOS sites (green = mountain, red = mountain valley, blue = Wasatch Front). Additional MOS site information available in Table 1.

Figure 2. Temperature MAE (°C) by site type for the 12-km MM5, 4-km MM5, 12-km MM5 adjusted using a standard atmosphere lapse rate, 4-km MM5 adjusted using a standard atmosphere lapse rate, and MOS. MAE averaged for all model runs and forecast hours (3–36).

Figure 3. Temperature a) MAE (°C) and b) BE (°C) by model run for the 12-km MM5, 4-km MM5, and MOS. Both 0000 and 1200 UTC initialized model runs included. MAE and BE for each model run averaged for all forecast hours (3–36).

Figure 4. Temperature MAE (°C) vs. observed mean diurnal temperature range (°C) for the a) 12-km MM5, b) 4-km MM5, and c) MOS. Linear trendlines are displayed for MAEs based on model temperatures (solid) and model temperatures adjusted to the actual elevation using a standard atmospheric lapse rate (dashed) in (a) and (b). MAE averaged for all forecast hours (3–36) and model runs.

Figure 5. Temperature a) MAE (°C) and b) BE (°C) by forecast hour for the 0000 and 1200 UTC initialized 12-km MM5, 4-km MM5, and MOS.

Figure 6. Dewpoint a) MAE (°C) and b) BE (°C) by model run for the 12-km MM5, 4-km MM5, and MOS. Both 0000 and 1200 UTC initialized model runs included. MAE and BE for each model run averaged for all forecast hours (3–36).

Figure 7. Dewpoint a) MAE (°C) and b) BE (°C) by forecast hour for the 0000 and 1200 UTC initialized 12-km MM5, 4-km MM5, and MOS.

Figure 8. Relative humidity MAE (%) by site type averaged for the 12-km MM5, 4-km MM5, and MOS. MAE averaged for all model runs and forecast hours (3–36).

Figure 9. Relative humidity a) MAE (%) and b) BE (%) by model run for the 12-km MM5, 4-km MM5, and MOS. Both 0000 and 1200 UTC initialized model runs included. MAE and BE for each model run averaged for all forecast hours (3–36).

Figure 10. Relative humidity a) MAE (%) and b) BE (%) by forecast hour for the 0000 and 1200 UTC initialized 12-km MM5, 4-km MM5, and MOS.

Figure 11. MAE for a) wind speed (m s^{-1}) and b) wind direction (°) by site type for the 12-km MM5, 4-km MM5, and MOS. MAE averaged for all model runs and forecast hours (3–36).

Figure 12. Wind speed a) MAE (m s^{-1}) and b) BE (m s^{-1}) by forecast hour for the 0000 and 1200 UTC initialized 12-km MM5, 4-km MM5, and MOS.

Figure 13. Wind speed MAE (m s^{-1}) vs. observed wind speed standard deviation (m s^{-1}) for the a) 12-km MM5, b) 4-km MM5, and c) MOS. MAE and observed standard deviation averaged for all model runs and forecast hours (3–36).

Figure 14. MAEs for (a) temperature (°C), (b) relative humidity (%), and (c) wind speed (m s^{-1}) by model run for the 12-km MM5, 4-km MM5, and MOS. Both 0000 and 1200 UTC initialized model runs included. MAE and BE for each model run averaged for the 36-h forecast projection.

Figure 15. 36-h temperature MAE (°C) for the 12-km MM5-Eta, 12-km MM5-AVN, MM5-Eta MOS, MM5-AVN MOS, and consensus MOS.

Figure 16. Temperature MAE (°C) at transportation corridor sites for the 12-km MM5, 4-km MM5, MOS, and Olympic Forecast Team forecasts issued at ~2300 (PM forecast) and ~1200 UTC (AM forecast). Validation period 3–25 Feb and 7–16 Mar 2002.

Figure 17. a) Temperature (°C), b) relative humidity (%), and c) wind speed (m s^{-1}) MAEs at outdoor venue sites for the 12-km MM5, 4-km MM5, MOS, and Olympic Forecast Team forecasts issued at ~0000 (PM forecast) and ~1200 UTC (AM forecast). Validation period 1–24 Feb 2002.

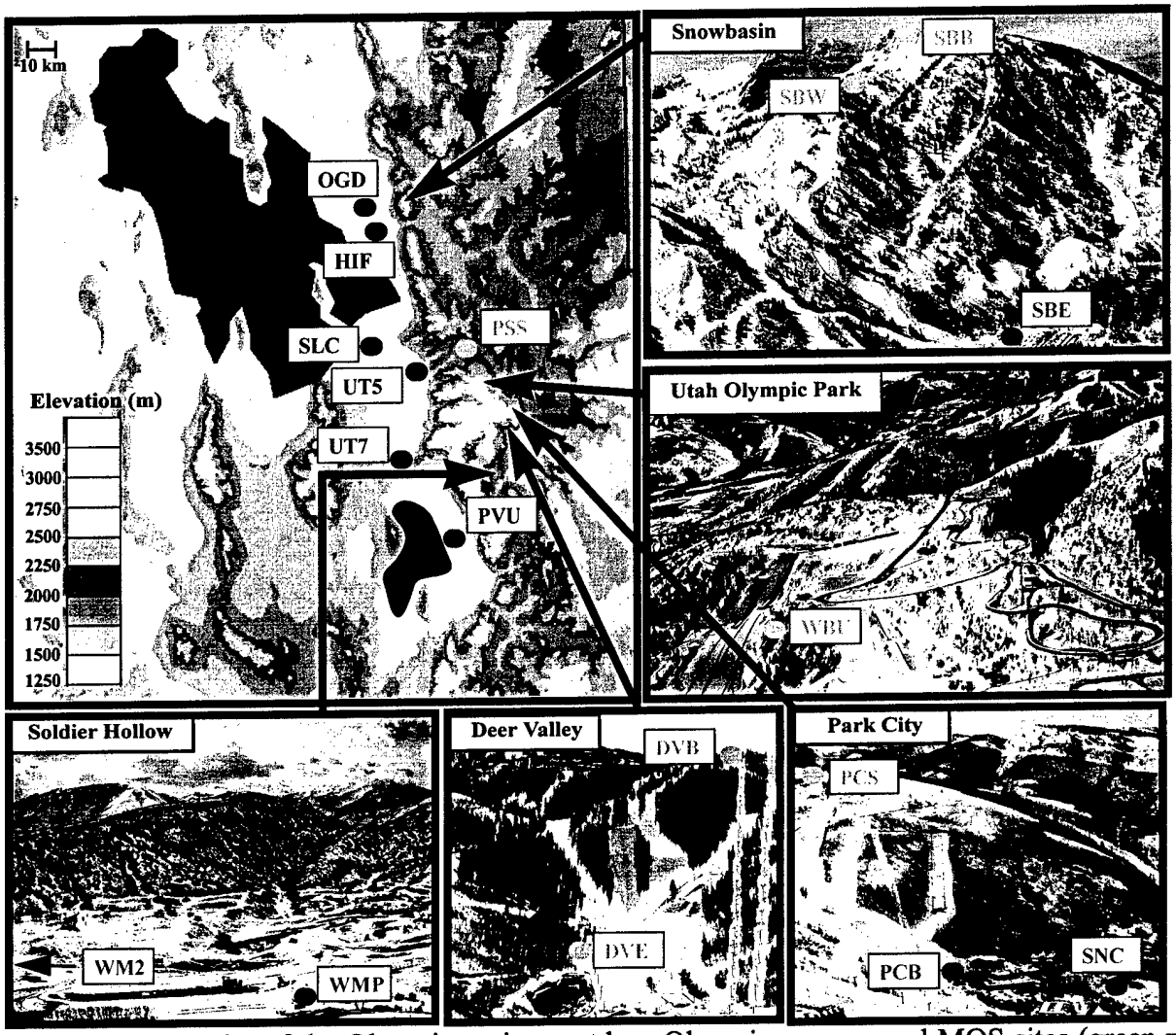

Figure 1. Geography of the Olympic region, outdoor Olympic venues, and MOS sites (green = mountain, red = mountain valley, blue = Wasatch Front). Additional MOS site information available in Table 1.

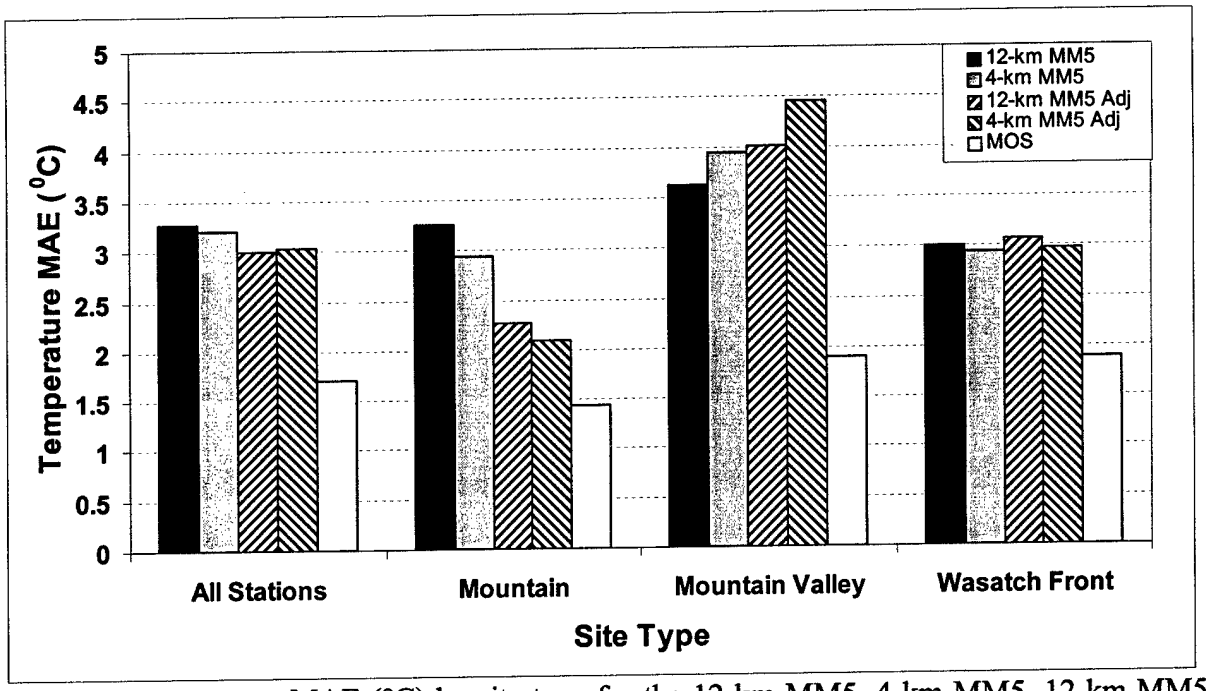

Figure 2. Temperature MAE (°C) by site type for the 12-km MM5, 4-km MM5, 12-km MM5 adjusted using a standard atmosphere lapse rate, 4-km MM5 adjusted using a standard atmosphere lapse rate, and MOS. MAE averaged for all model runs and forecast hours (3–36).

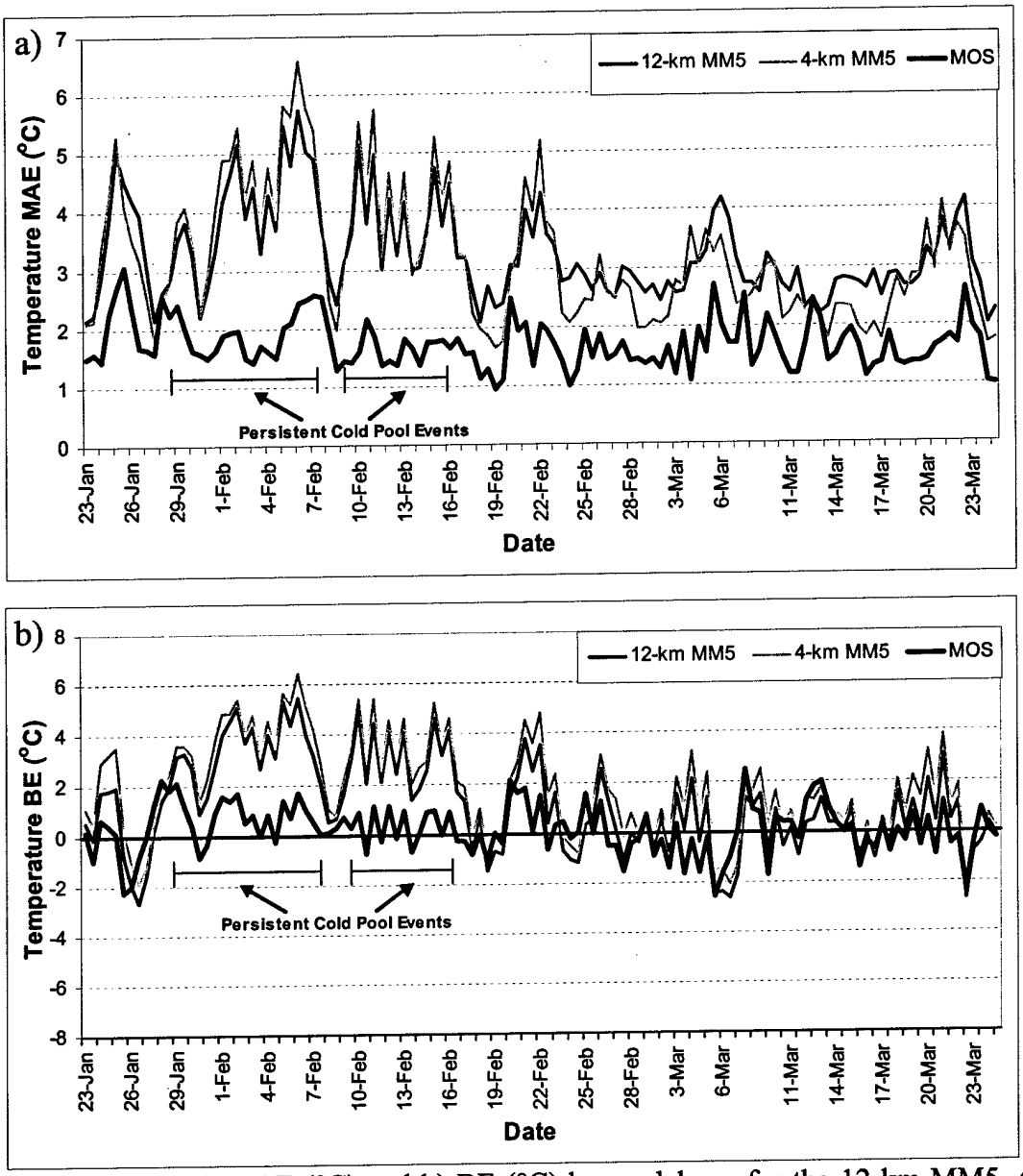

Figure 3. Temperature a) MAE (°C) and b) BE (°C) by model run for the 12-km MM5, 4-km MM5, and MOS. Both 0000 and 1200 UTC initialized model runs included. MAE and BE for each model run averaged for all forecast hours (3–36).

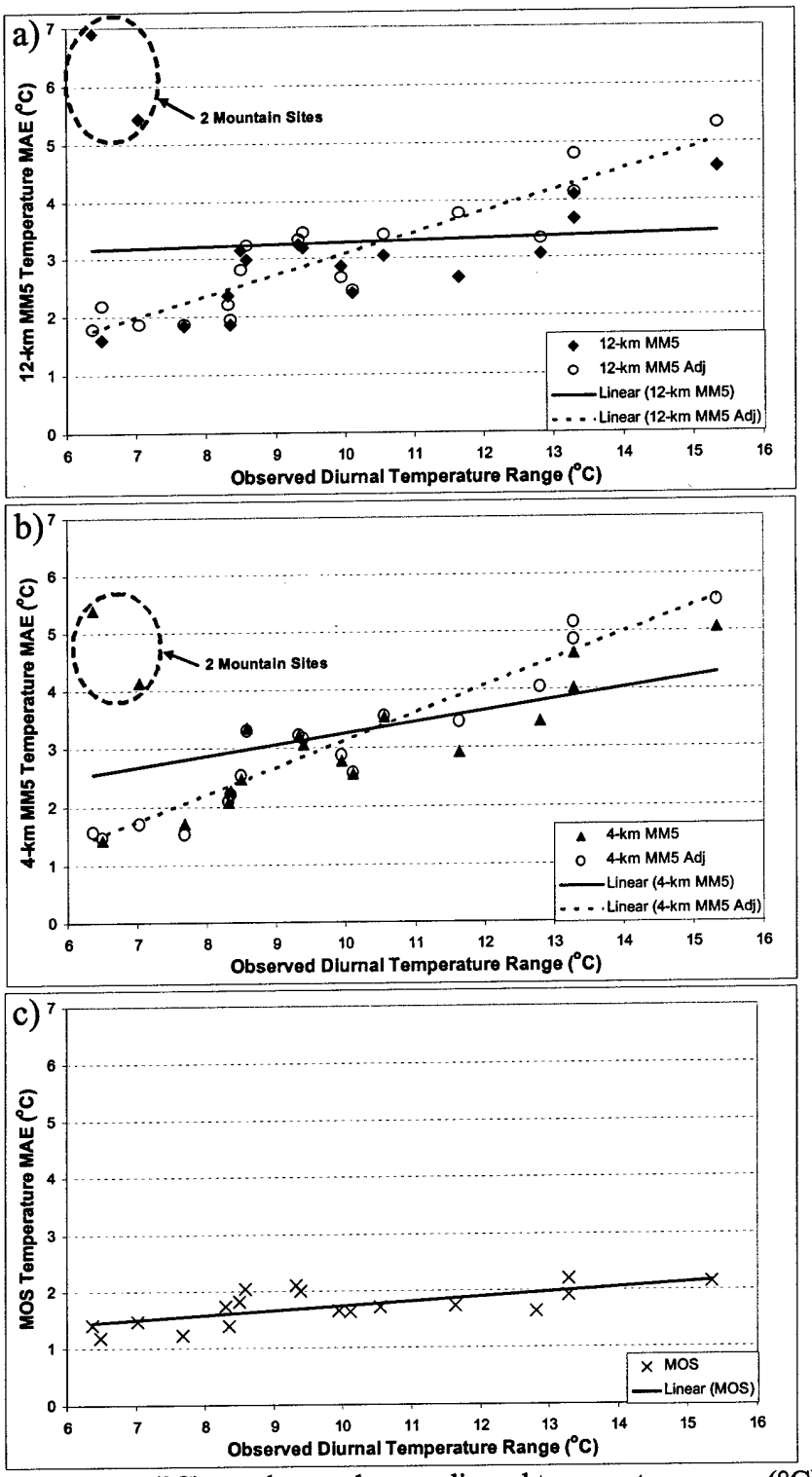

Figure 4. Temperature MAE (°C) vs. observed mean diurnal temperature range (°C) for the a) 12-km MM5, b) 4-km MM5, and c) MOS. Linear trendlines are displayed for MAEs based on model temperatures (solid) and model temperatures adjusted to the actual elevation using a standard atmospheric lapse rate (dashed) in (a) and (b). MAE averaged for all forecast hours (3–36) and model runs.

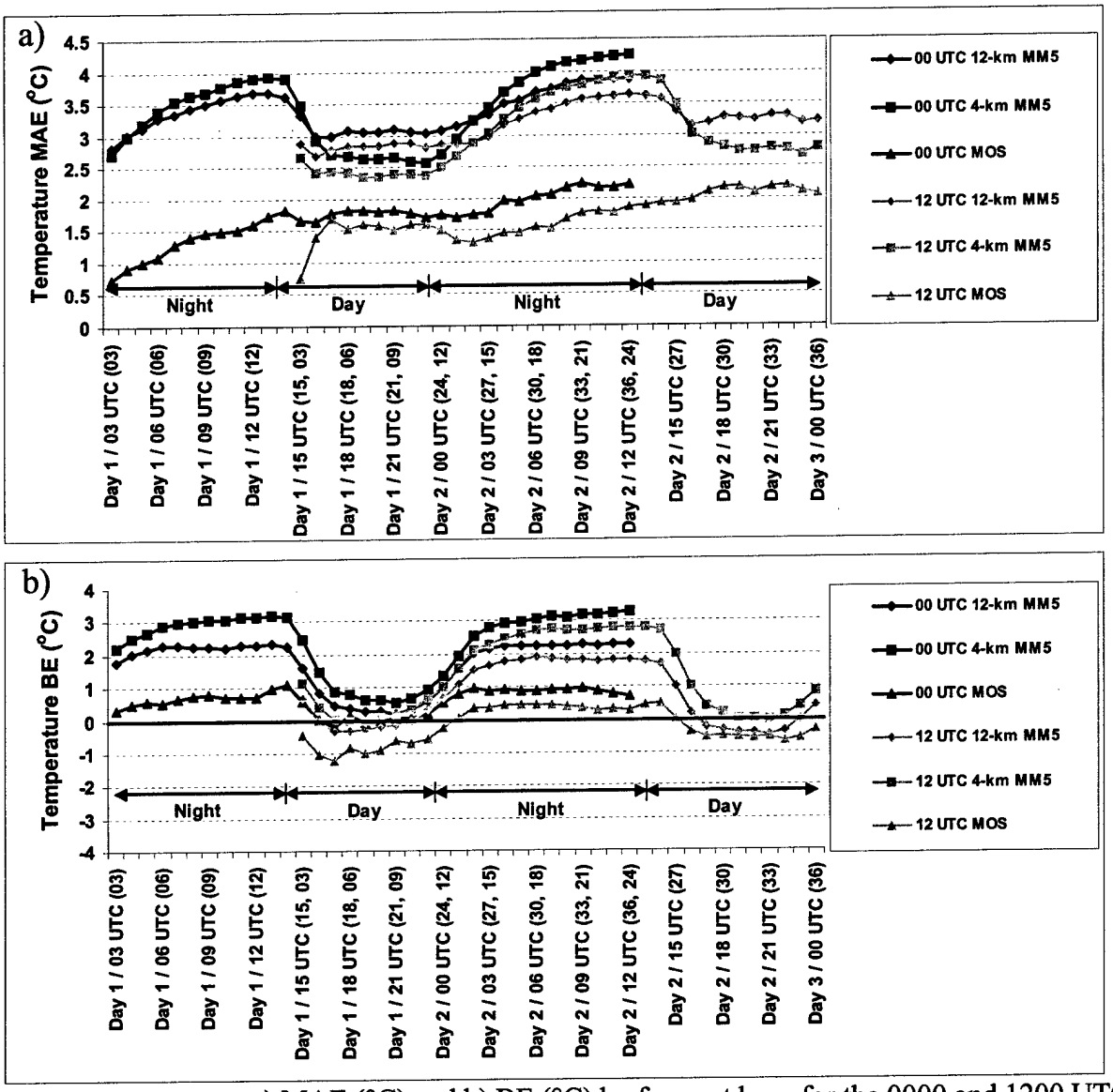

Figure 5. Temperature a) MAE (°C) and b) BE (°C) by forecast hour for the 0000 and 1200 UTC initialized 12-km MM5, 4-km MM5, and MOS.

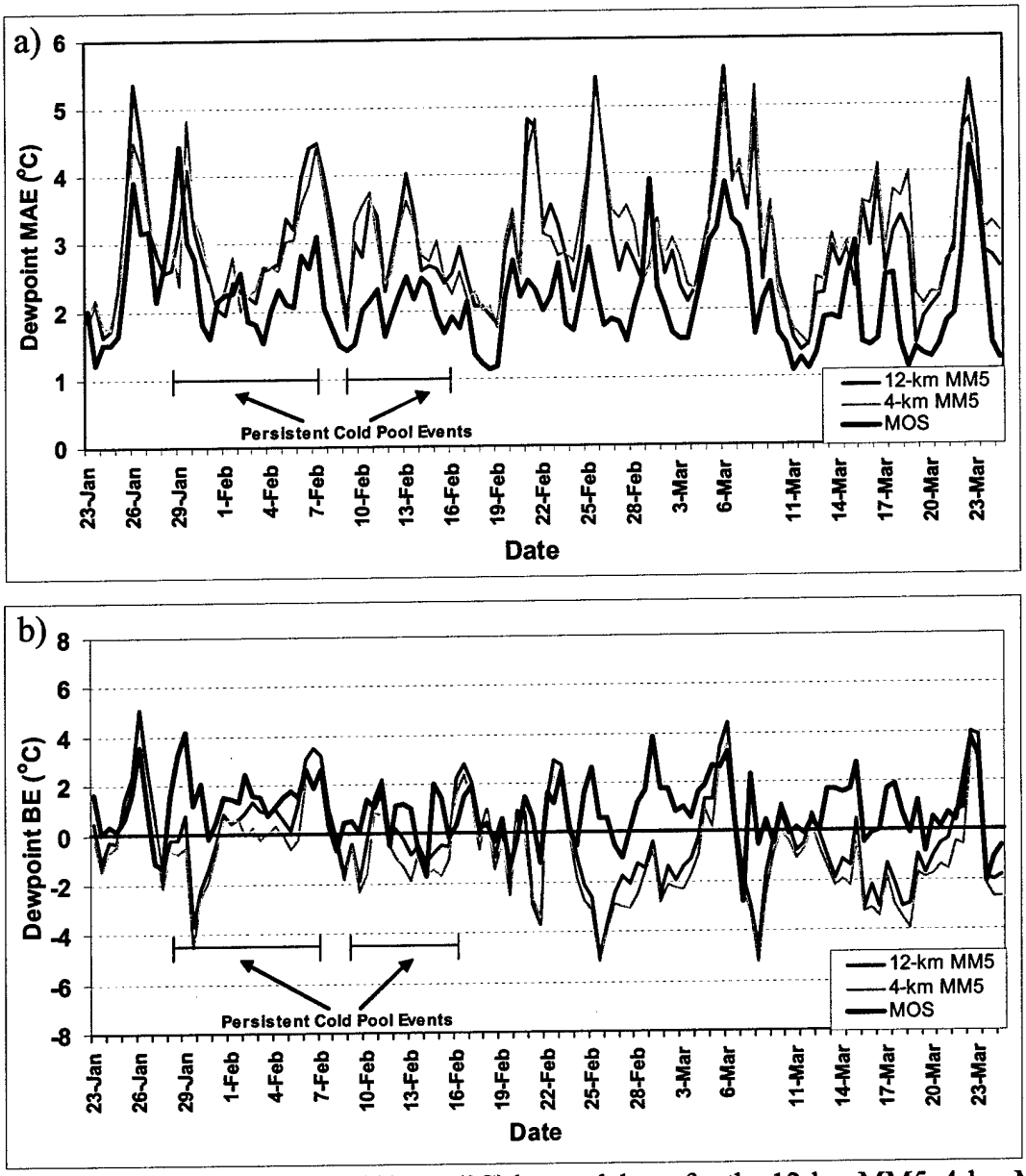

Figure 6. Dewpoint a) MAE (°C) and b) BE (°C) by model run for the 12-km MM5, 4-km MM5, and MOS. Both 0000 and 1200 UTC initialized model runs included. MAE and BE for each model run averaged for all forecast hours (3–36).

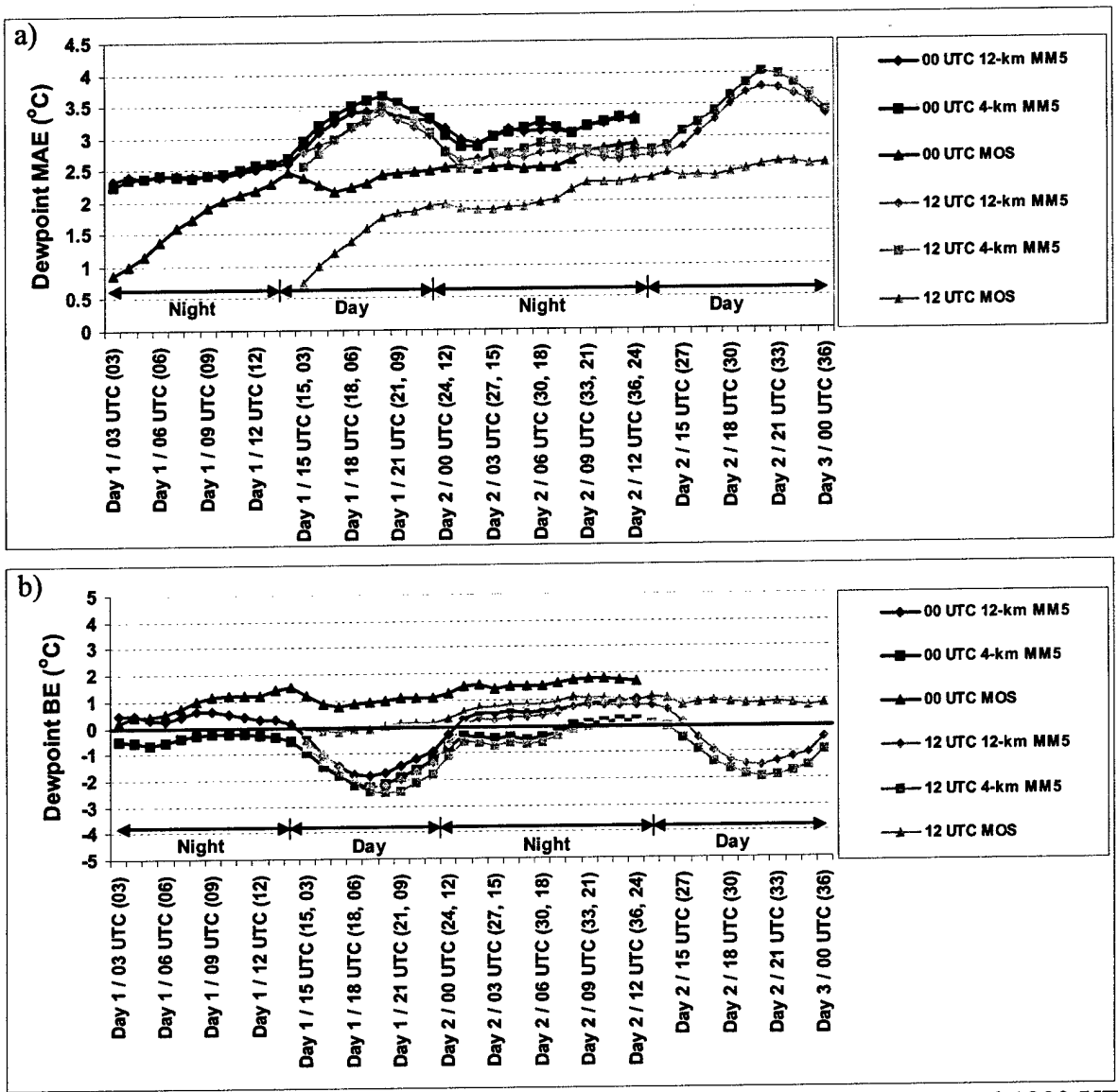

Figure 7. Dewpoint a) MAE (°C) and b) BE (°C) by forecast hour for the 0000 and 1200 UTC initialized 12-km MM5, 4-km MM5, and MOS.

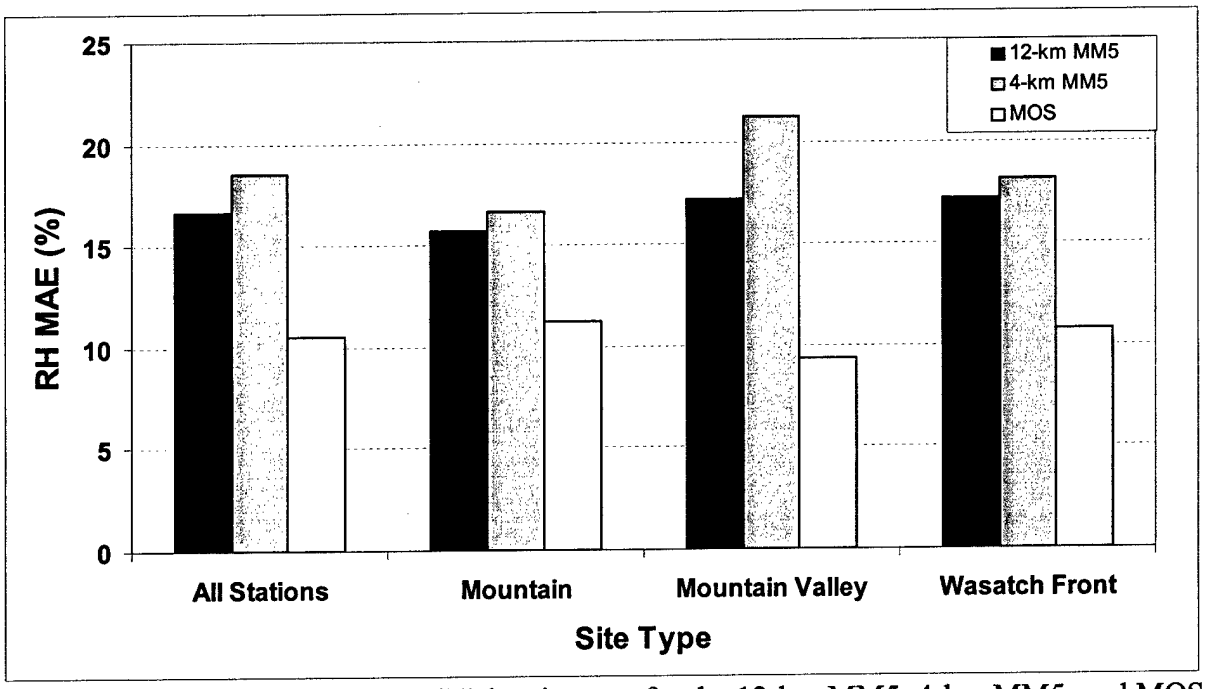

Figure 8. Relative humidity MAE (%) by site type for the 12-km MM5, 4-km MM5, and MOS. MAE averaged for all model runs and forecast hours (3–36).

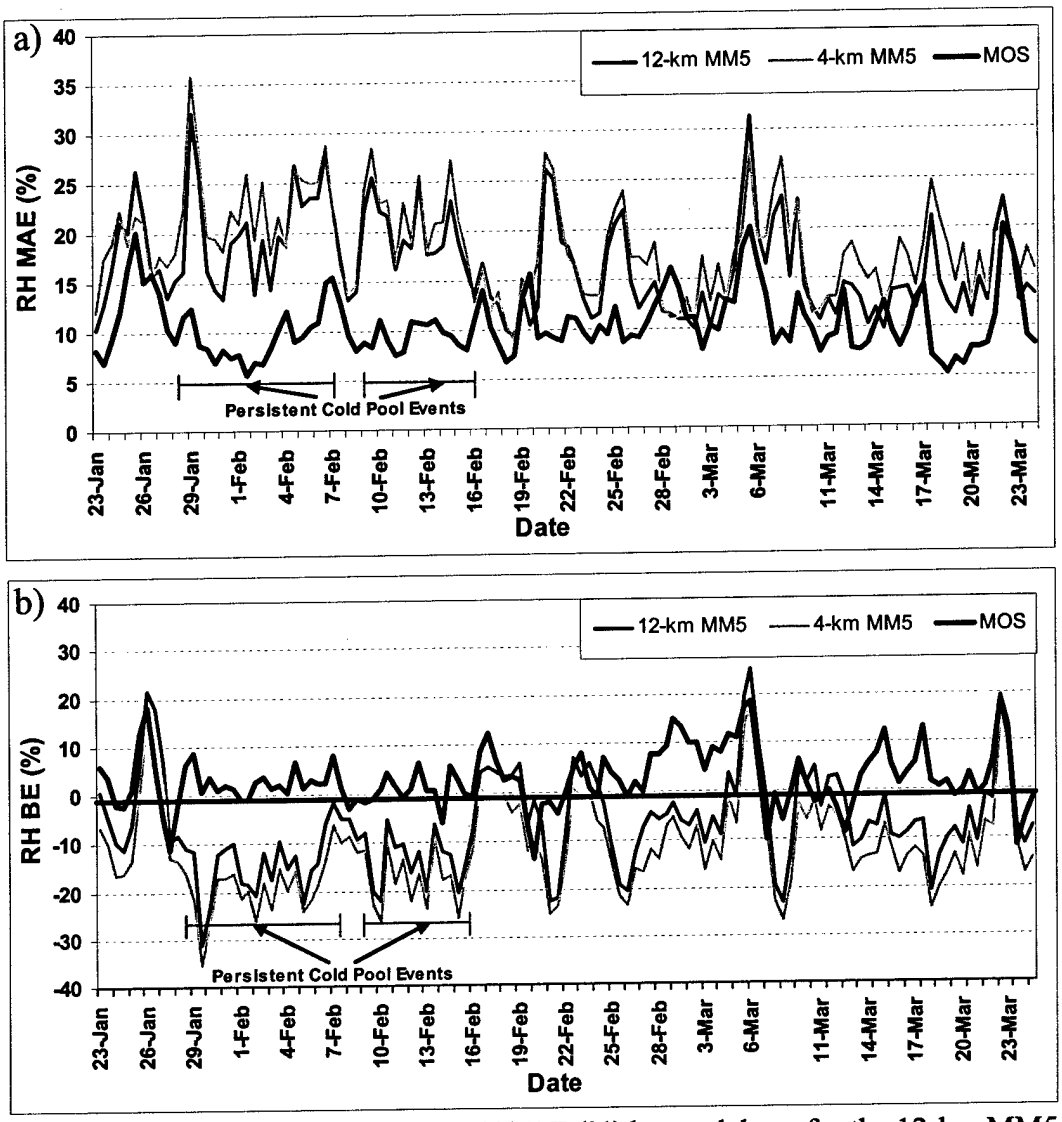

Figure 9. Relative humidity a) MAE (%) and b) BE (%) by model run for the 12-km MM5, 4-km MM5, and MOS. Both 0000 and 1200 UTC initialized model runs included. MAE and BE for each model run averaged for all forecast hours (3–36).

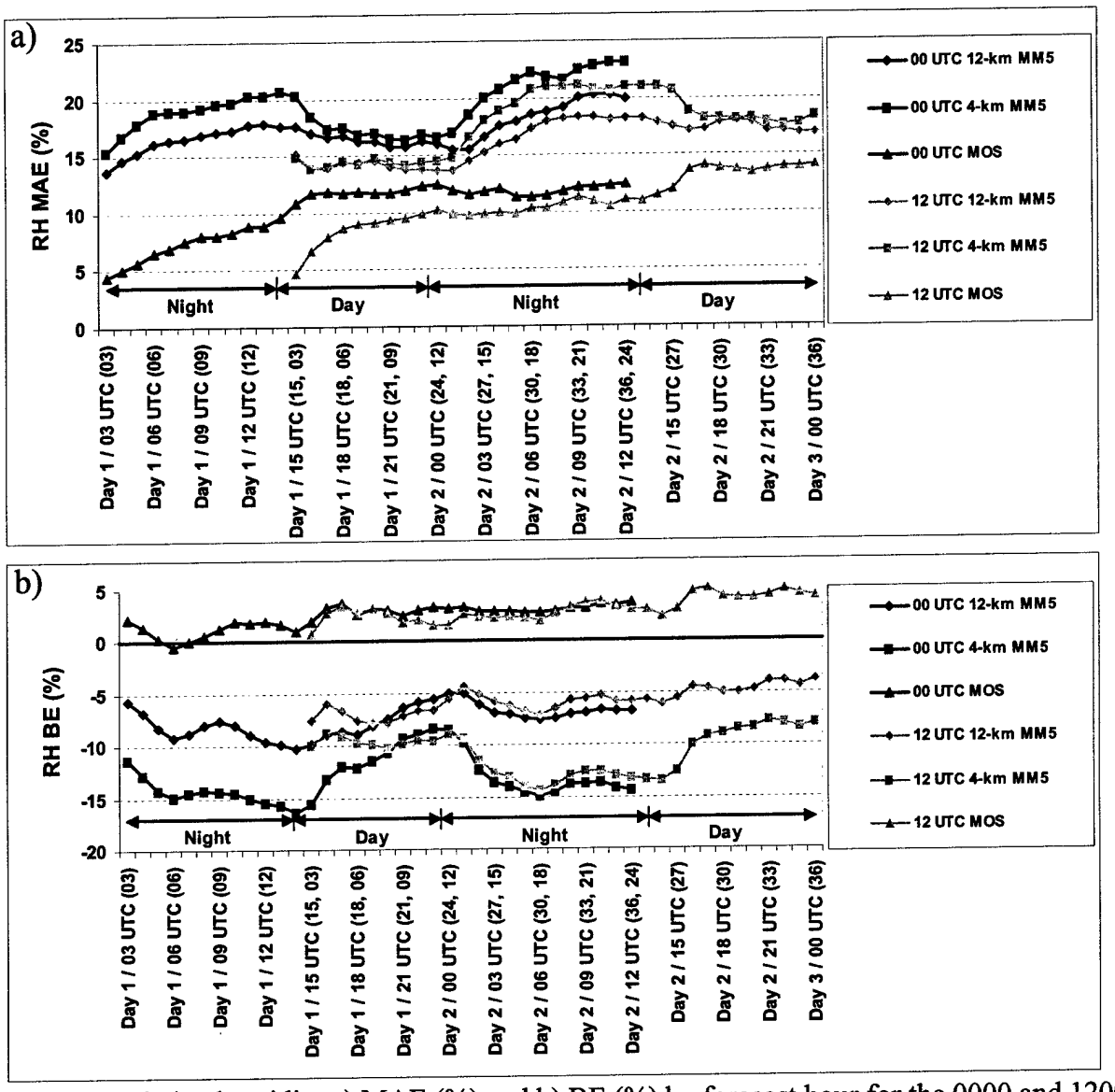

Figure 10. Relative humidity a) MAE (%) and b) BE (%) by forecast hour for the 0000 and 1200 UTC initialized 12-km MM5, 4-km MM5, and MOS.

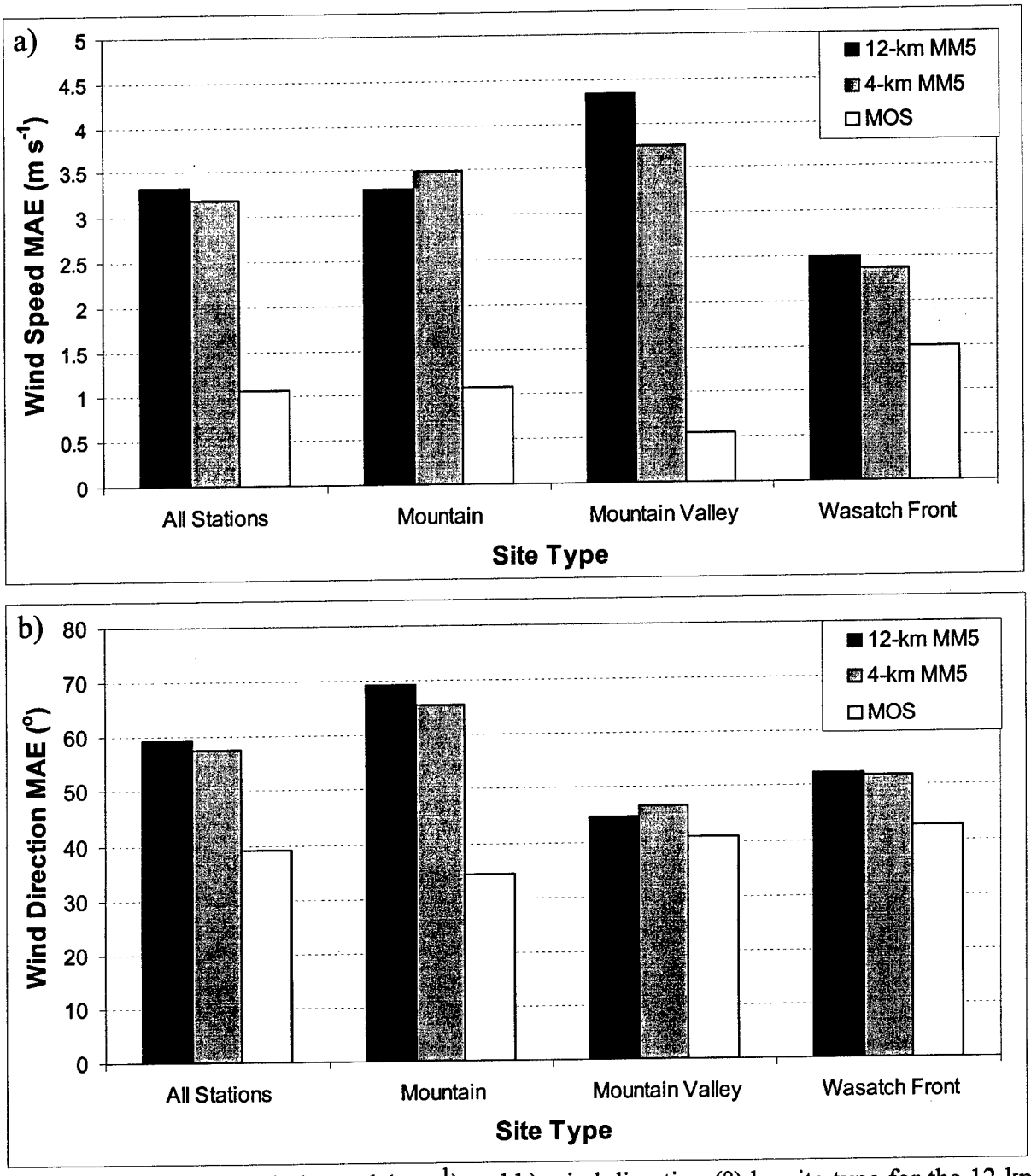

Figure 11. MAE for a) wind speed (m s^{-1}) and b) wind direction (°) by site type for the 12-km MM5, 4-km MM5, and MOS. MAE averaged for all model runs and forecast hours (3–36).

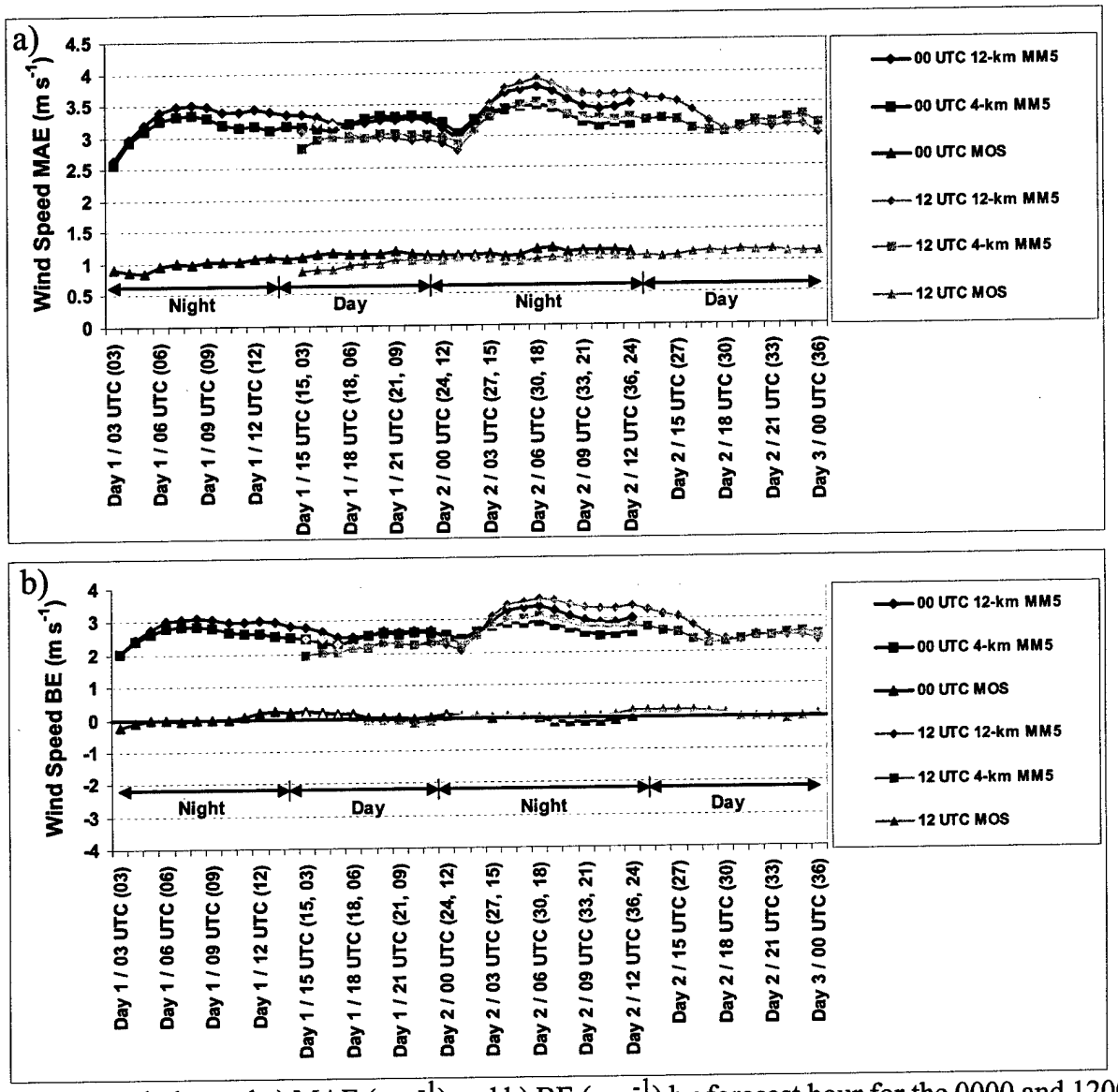

Figure 12. Wind speed a) MAE (m s^{-1}) and b) BE (m s^{-1}) by forecast hour for the 0000 and 1200 UTC initialized 12-km MM5, 4-km MM5, and MOS.

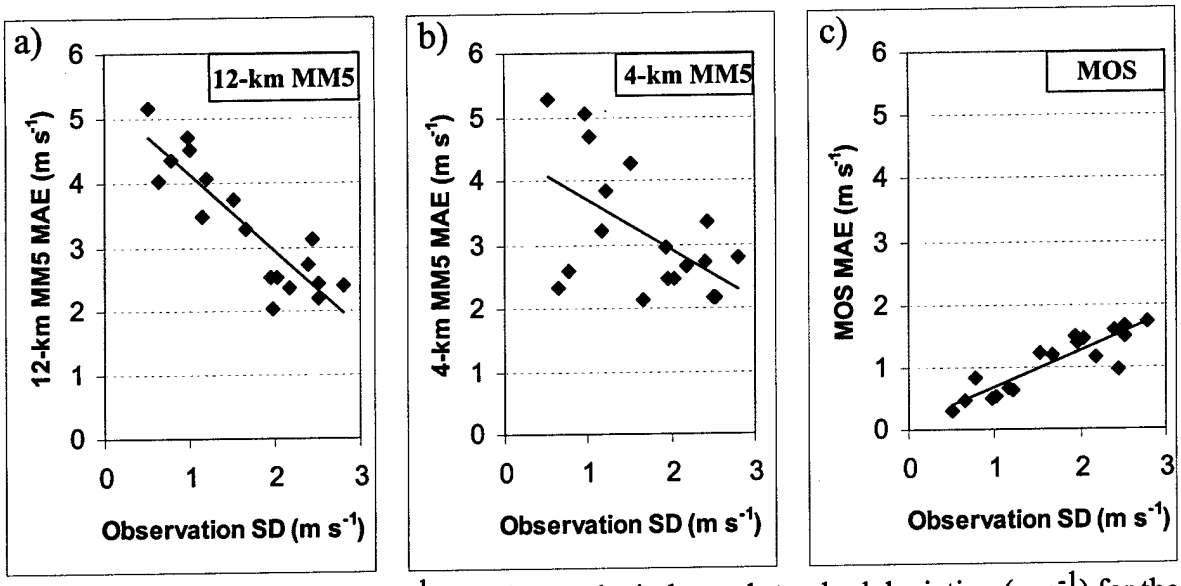

Figure 13. Wind speed MAE (m s^{-1}) vs. observed wind speed standard deviation (m s^{-1}) for the a) 12-km MM5, b) 4-km MM5, and c) MOS. MAE and observed standard deviation averaged for all model runs and forecast hours (3–36).

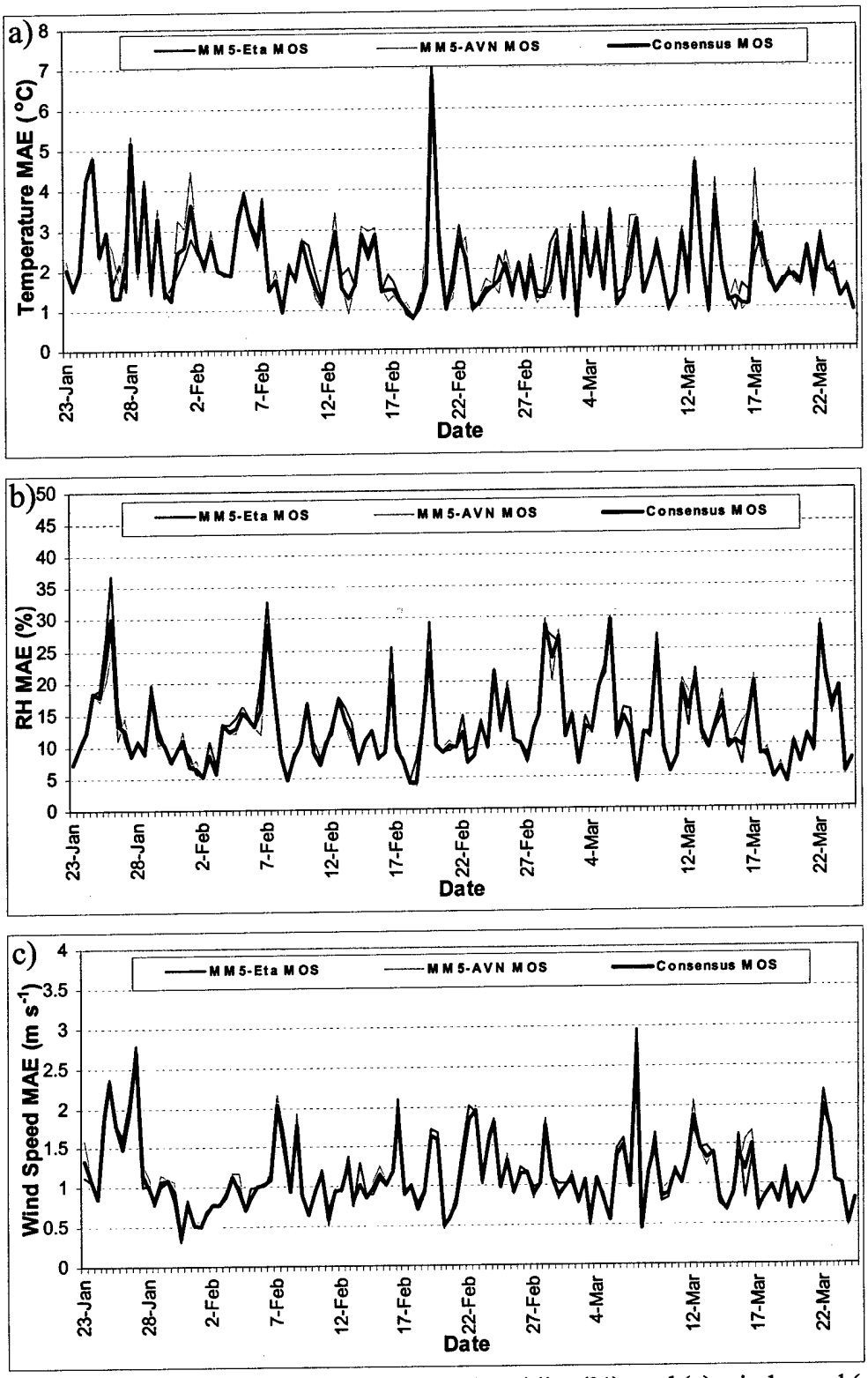

Figure 14. MAE for (a) temperature (°C), (b) relative humidity (%), and (c) wind speed (m s^{-1}) by model run for the 12-km MM5, 4-km MM5, and MOS. Both 0000 and 1200 UTC initialized model runs included. MAE and BE for each model run averaged for the 36-h forecast projection.

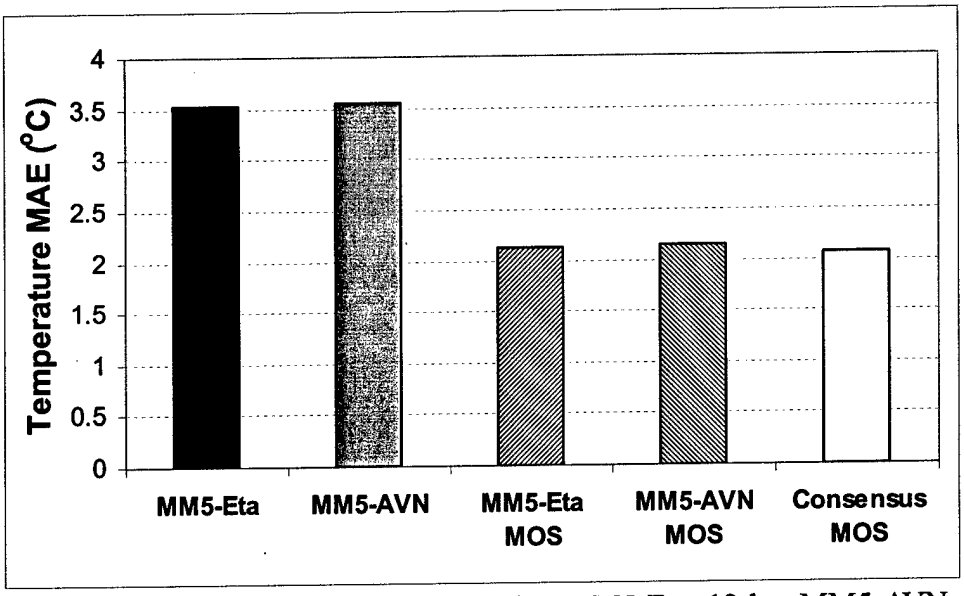

Figure 15. 36-h temperature MAE (°C) for the 12-km MM5-Eta, 12-km MM5-AVN, MM5-Eta MOS, MM5-AVN MOS, and consensus MOS.

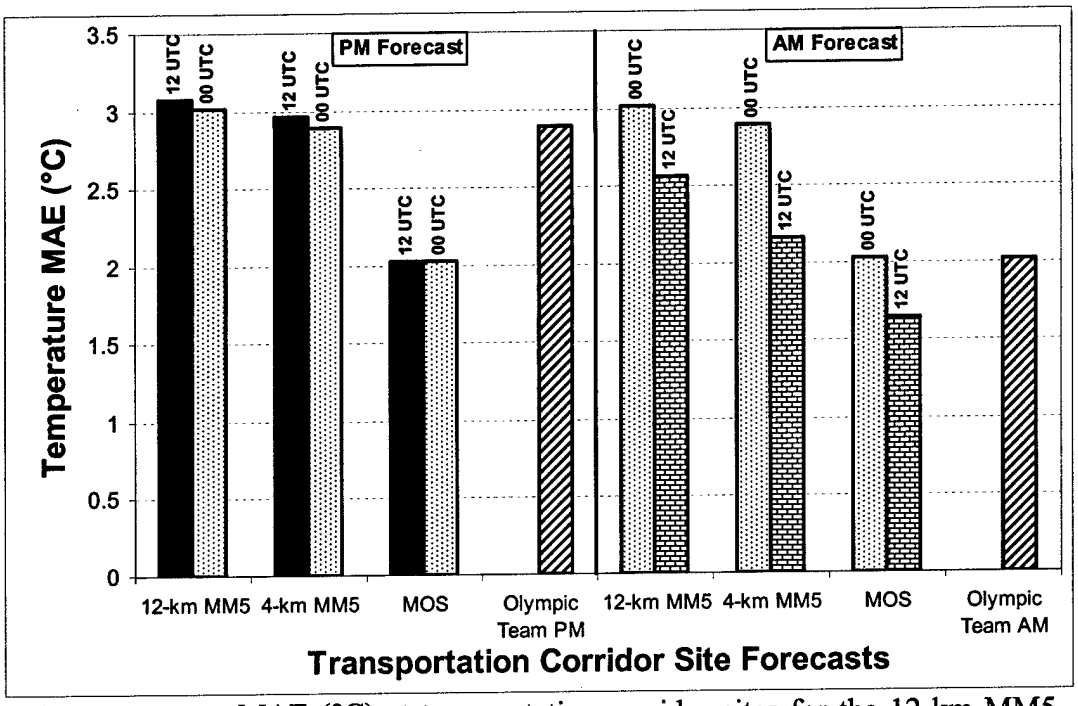

Figure 16. Temperature MAE (°C) at transportation corridor sites for the 12-km MM5, 4-km MM5, MOS, and Olympic Forecast Team forecasts issued at ~2300 (PM forecast) and ~1200 UTC (AM forecast). Validation period 3–25 Feb and 7–16 Mar 2002.

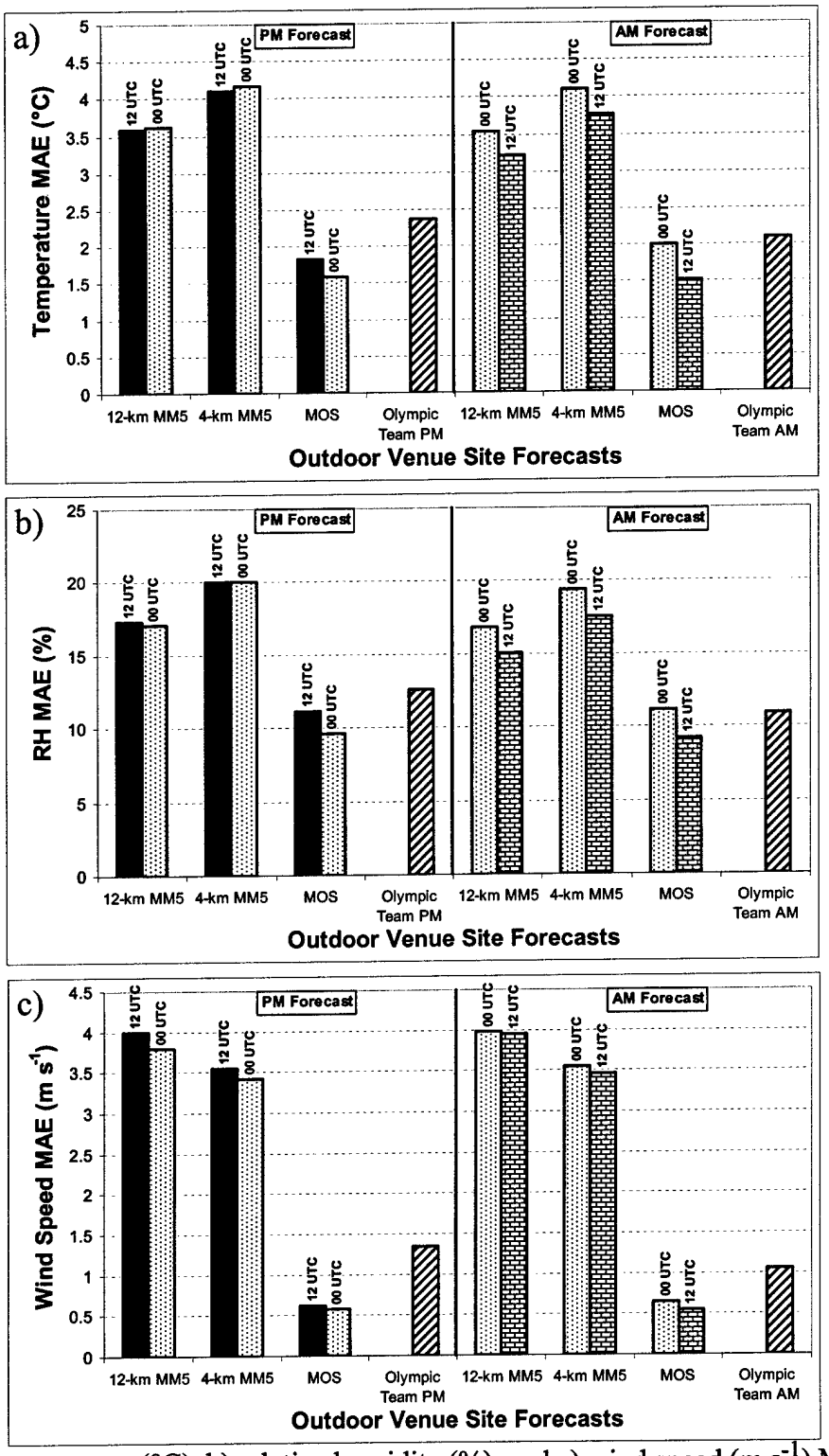

Figure 17. a) Temperature (°C), b) relative humidity (%), and c) wind speed (m s^{-1}) MAEs at outdoor venue sites for the 12-km MM5, 4-km MM5, MOS, and Olympic Forecast Team forecasts issued at ~0000 (PM forecast) and ~1200 UTC (AM forecast). Validation period 1–24 Feb 2002.